medRxiv preprint doi: https://doi.org/10.1101/2022.09.17.22280033; this version posted February 22, 2023. The copyright holder for this preprint (which was not certified by peer review) is the author/funder, who has granted medRxiv a license to display the preprint in perpetuity. All rights reserved. No reuse allowed without permission.

Age-Associated B cells predict impaired humoral immunity after COVID-19 vaccination in patients receiving immune checkpoint blockade

Juan Carlos Yam-Puc[1]†*, Zhaleh Hosseini[1]†, Emily C. Horner[1]†, Pehuén Pereyra Gerber[2,3]†, Nonantzin Beristain-Covarrubias[1]†, Robert Hughes[1]†, Aleksei Lulla[4], Maria Rust[1], Rebecca H. Boston[1], Magda Ali[1], Katrin Fischer[4], Edward Simmons-Rosello[1], Martin O'Reilly[1], Harry Robson[1], Lucy H. Booth[1], Lakmini Kahanawita[1], Andrea Correa-Noguera[5], Lourdes Ceron-Gutierrez[5], Baerbel Keller[6,7], Andrew Craxton[1], Georgina S.F. Anderson[1], Xiao-Ming Sun[1], Anne Elmer[8], Caroline Saunders[8], Areti Bermperi[8], Sherly Jose[8], Nathalie Kingston[9], Thomas Mulroney[1], CITIID-NIHR COVID-19 BioResource Collaboration, Mike Chapman[1], Sofia Grigoriadou[10], Marion MacFarlane[1], Anne E. Willis[1], Kiran R. Patil[1], Sarah Spencer[1], Emily Staples[1], Klaus Warnatz[6,7,11] , Matthew S. Buckland[10,12], Florian Hollfelder[4], Marko Hyvönen[4], Rainer Döffinger[5], Christine Parkinson[5§], Sara Lear[5§], Nicholas J. Matheson[2,3,5,13§], James E. D. Thaventhiran[1,5§*].

[1] Medical Research Council Toxicology Unit, School of Biological Sciences, University of Cambridge, Cambridge, UK.

[2] Cambridge Institute of Therapeutic Immunology and Infectious Disease (CITIID), University of Cambridge, Cambridge, UK

[3] Department of Medicine, University of Cambridge, Cambridge, UK

[4] Department of Biochemistry, University of Cambridge, Cambridge, UK

[5] Department of Clinical Immunology, Cambridge University NHS Hospitals Foundation Trust, Cambridge, UK

[6] Department of Rheumatology and Clinical Immunology, Medical Center - University of Freiburg, Faculty of Medicine, University of Freiburg, Freiburg, Germany.

[7] Center for Chronic Immunodeficiency (CCI), Medical Center - University of Freiburg, Faculty of Medicine, University of Freiburg, Freiburg, Germany.

[8] NIHR Cambridge Clinical Research Facility, Cambridge, UK

[9] NIHR BioResource, Cambridge University Hospitals NHS Foundation Trust, Cambridge, UK

[10] Department of Clinical Immunology, Barts Health, London, UK

[11] Department of Immunology, University Hospital Zurich, Zurich, Switzerland

[12] UCL GOSH Institute of Child Health Division of Infection and Immunity, Section of Cellular and Molecular Immunology, London, UK

[13] NHS Blood and Transplant, Cambridge, UK

† These authors contributed equally

NOTE: This preprint reports new research that has not been certified by peer review and should not be used to guide clinical practice.

medRxiv preprint doi: https://doi.org/10.1101/2022.09.17.22280033; this version posted February 22, 2023. The copyright holder for this preprint (which was not certified by peer review) is the author/funder, who has granted medRxiv a license to display the preprint in perpetuity. All rights reserved. No reuse allowed without permission.

§ These authors contributed equally

* Corresponding authors: jedt2@cam.ac.uk, jcy28@cam.ac.uk.

Key words: Age-associated B cells (ABCs), Inborn error of immunity (IEI), immune-checkpoint blockade, neutralising antibodies, antigen-specific memory B cells, BNT162b2 vaccine, immunodeficiency, cancer

medRxiv preprint doi: https://doi.org/10.1101/2022.09.17.22280033; this version posted February 22, 2023. The copyright holder for this preprint (which was not certified by peer review) is the author/funder, who has granted medRxiv a license to display the preprint in perpetuity. All rights reserved. No reuse allowed without permission.

Abstract

Age-associated B cells (ABCs) accumulate with age, as well as in individuals with a range of immunological dyscrasias. These include patients with cancer treated with immune checkpoint blockade and patients with inborn errors of immunity. In this study, we sought to determine whether ABCs found in all these conditions are similar, and whether they enhance or detract from the response to COVID-19 vaccination. We use single cell RNA sequencing to show that ABCs arising from distinct aetiologies have common transcriptional profiles and may be subdivided according to the expression of genes associated with different immune functions, such as the autoimmune regulator (AIRE). Next, we perform detailed longitudinal profiling of the COVID-19 vaccination response in patients and controls. We show that high pre-vaccination ABC frequency correlates with decreased levels of antigen-specific memory B cells, and reduced magnitude and longevity of neutralising capacity against SARS-CoV-2 virus. Potentially contributing to this, ABCs express high levels of the inhibitory FcγRIIB receptor and are distinctive in their ability to bind immune complexes. This could contribute to diminished vaccine responses either directly as result of inhibitory signalling or indirectly via enhanced clearance of immune complexed-antigen. Expansion of ABCs may therefore serve as a biomarker identifying individuals at risk of a suboptimal response to COVID-19 vaccination.

medRxiv preprint doi: https://doi.org/10.1101/2022.09.17.22280033; this version posted February 22, 2023. The copyright holder for this preprint (which was not certified by peer review) is the author/funder, who has granted medRxiv a license to display the preprint in perpetuity. All rights reserved. No reuse allowed without permission.

Introduction

Despite the success of mRNA-lipid nanoparticle (mRNA-LNP) COVID-19 vaccines in reducing the risk of symptomatic infection, hospitalisation, and death[1,2], vaccinated patients with cancer remain at increased risk of severe outcomes following SARS-CoV-2 infection[3]. Immune checkpoint blockade (ICB) is a cancer therapy that observational studies[4-6] suggest could improve the efficacy of vaccines. By targeting PD-1 and CTLA-4 checkpoints, ICB non-specifically promotes T cell responses, including those involved in anti-viral and anti-cancer immunity. Furthermore, preclinical evidence indicates immune checkpoint blockade can, via T and B cell interactions, enhance antibody responses[7,8]. The neutralising antibodies produced by the humoral response are a vital component of vaccine protection as they inhibit viral replication *in vitro* and correlate with protection against infection *in vivo*[9-11]. However, complicating the positive potential of ICB for vaccine enhancement, ICB induces the expansion of a B cell subset termed in other contexts Age-Associated B cells (ABCs)[12], which may have a confounding effect on humoral vaccine responses.

ABCs comprise a naturally occurring population of antigen-experienced B cells which expands continuously with age in healthy individuals but accumulates prematurely in people with certain immune dyscrasias, autoimmunity, and/or infectious diseases[13]. They have also been termed $CD21^{low}$ B cells, $CD11c^{+}$ B cells, $CD11c^{+}$T-bet^{+} B cells, double negative 2 (DN2) B cells or atypical memory B cells[13-20], and may additionally be generated by external challenges[21,22], including COVID-19 infection and vaccination[23]. Although ABCs are associated with disease in autoimmunity, their role in vaccine immunity is uncertain. In mice, these cells are required for optimal antibody responses following influenza vaccination[24], possibly due to enhanced ability to present antigens to T cells relative to follicular B cells[16,25]. In patients with cancer treated with ICB, the expansion of ABCs precedes the development of both antibody-mediated and non-antibody-mediated autoimmunity[12]. This is in keeping with their role in promoting antibody responses. However, we and others have shown that expansion of ABCs is associated with antibody deficiency in specific cohorts of patients with inborn errors of immunity (IEI)[26-30]. These include patients with *NFKB1* haploinsufficiency, in whom the genetic lesion leads to a combined B and T cell defect[29], and patients with *CTLA4* haploinsufficiency, in whom the genetic-lesion leads predominantly to a B cell-extrinsic functional T cell deficit [27,31]. These observations suggest two key questions: are the ABCs found in patients treated with ICB equivalent to those found in other settings? And do these

medRxiv preprint doi: https://doi.org/10.1101/2022.09.17.22280033; this version posted February 22, 2023. The copyright holder for this preprint (which was not certified by peer review) is the author/funder, who has granted medRxiv a license to display the preprint in perpetuity. All rights reserved. No reuse allowed without permission.

cells, when expanded through distinct mechanisms, have a positive or negative effect on humoral vaccine responses?

The increase in patients with cancer eligible to receive ICB treatment[32] and the survival benefit conferred by ICB treatment means that optimally protecting patients with cancer who are receiving these therapies from infection will be an increasing priority. Here, we address the above questions regarding the characteristics and activity of ABCs in different patient groups as well as developing an understanding of the crosstalk between ICB and successful vaccination.

Results

ABCs arising from distinct aetiologies have common transcriptional profiles

We first assessed the similarities between ABCs from patients with different causes for ABC expansion, using single cell RNA sequencing (scRNAseq). This included B cells from healthy controls (HC, n=8), patients with cancer treated with ICB (ICB, n=8) and patients with *NFKB1* or *CTLA4* haploinsufficiency (IEI, n=4), together with a published set of single B cell transcriptomes from patients with systemic lupus erythematosus (SLE, n=3)[33]. By focussing on patients with rare, monogenic defects leading to well-characterised IEI, we were able to ensure that contrasting B cell intrinsic (*NFKB1*) and extrinsic (*CTLA4*) aetiologies were included. Unsupervised clustering of the 52,402 B cells, displayed in a uniform manifold approximation and projection (UMAP) visualisation, revealed six clusters (**Fig. 1a).** Using CITE-seq, we identified ABCs that had low CD21 and high CD11c surface protein expression, in keeping with the definitions used in some previous flow cytometry-based studies[16,34] (**Supplementary Fig. 1a-b**). Cells were dispersed across all clusters regardless of the patient group or sex from which they originated (**Fig. 1b-d)**. ABC frequencies were higher in all patient groups compared to healthy controls (**Fig. 1d).**

Distinct subsets of ABCs express genes associated with distinct immune functions

The clustering and marker gene expression suggested that the ABC population can be subdivided into “Classical ABCs”, “Anergic ABCs” and “CD1c ABCs” (**Fig. 1e).** Classical ABC frequencies were higher in females and patients with SLE (**Fig. 1b-d** and **Supplementary Fig. 1c-f**). ABCs have been described as “anergic B cells” [35,36]. Interestingly, anergic ABCs (expressing canonical genes associated with anergy, such as *EGR1* and *NR4A1*) clustered separately from Classical ABCs (**Fig. 1a and Fig. 1e** and **Supplementary Table 1**), indicating heterogeneity within ABCs for this phenotype. Indeed,

medRxiv preprint doi: https://doi.org/10.1101/2022.09.17.22280033; this version posted February 22, 2023. The copyright holder for this preprint (which was not certified by peer review) is the author/funder, who has granted medRxiv a license to display the preprint in perpetuity. All rights reserved. No reuse allowed without permission.

many of the most differentially expressed genes in Classical ABCs were associated with MHC class II-restricted antigen presentation (**Fig. 1f**). Gene ontology enrichment analysis demonstrated selective upregulation of biological processes associated with professional antigen presentation, such as antigen uptake, processing, class II presentation, and co-stimulation (**Fig. 1g** and **Supplementary Table 2**). This was specific for MHC class-II-restricted antigen presentation, as genes required for MHC class I-restricted antigen presentation were instead differentially expressed in CD1c ABCs, relative to Classical ABCs (**Supplementary Fig. 2**). This supports the functional separation of these two clusters, which were less distinct on UMAP visualisation (**Fig. 1a)**. To further analyse these different clusters, we used single cell BCR sequencing data to calculate the vertex/node Gini index as a measure of clonal expansion[37] and the degree index from dandelion[38,39] as a measure of how cells are clonally related. The classical ABC cluster had the highest Gini index and second highest degree index, suggesting that more clones of classical ABCs are expanded and that these cells are clonally related (**Supplementary Fig. 3**).

Upregulation of AIRE and its target genes is seen in Classical ABCs

Consistent with our gene ontology analysis, we confirmed MHC-II antigen presentation related genes, such as HLA-proteins, *CD74* and *CD86*, were amongst the most differentially expressed genes of Classical ABCs. Additionally, other important genes involved in the processing of peptides, oligosaccharides and fatty acids such as *LGMN, IFI30, PSAP* and *ASAH1* were differentially expressed (**Fig. 2a** and **Supplementary Table 3**). Intriguingly, this analysis also revealed the Autoimmune Regulator (*AIRE*) to be significantly upregulated in Classical ABCs from all subject cohorts (**Fig. 2a-b, Supplementary Fig. 4**). *AIRE*-expressing B lymphocytes were also in other clusters, albeit at a much lower frequency (**Fig. 2c**). This is consistent with the accumulation of AIRE-expressing B cells in the Classical ABC differentiation state during peripheral B cell development, rather than selective upregulation of AIRE after ABC differentiation. Expression of a single gene in 3.85% of cells within a subset will make a negligible contribution to the UMAP clustering, therefore enrichment of *AIRE*-expressing cells within the apex of the Classical ABC cluster (**Supplementary Fig. 4a)** further supports the biological association of AIRE expression and ABC differentiation. AIRE is a transcriptional regulator expressed in both the thymic epithelium and thymic B cells[40,41], which increases expression of tissue-restricted antigens (TRAs). TRA expression in the thymus is a central tolerance mechanism, whereby stimulation of developing T cells by antigens usually expressed in non-thymic tissues directs these cells away from fates with the potential for harmful self-antigen driven autoimmune responses. Previous reports have suggested that AIRE is not functional in the small

medRxiv preprint doi: https://doi.org/10.1101/2022.09.17.22280033; this version posted February 22, 2023. The copyright holder for this preprint (which was not certified by peer review) is the author/funder, who has granted medRxiv a license to display the preprint in perpetuity. All rights reserved. No reuse allowed without permission.

proportion of peripheral lymphocytes in which it can be detected[42-44], although AIRE function has never been assessed in ABCs (a peripheral B cell subset specifically associated with autoimmune disease[16,45,46]). *AIRE*-expressing cells also upregulated a set of genes previously defined as AIRE targets in thymic B cells[41], which are predominantly expressed in other tissues such as brain (**Fig. 2d**, **Supplementary Table 4 and Supplementary Fig. 5**). In addition, Classical ABCs upregulated HLA-G (**Supplementary Fig. 2**), a non-classical class I HLA molecule transactivated by AIRE in thymic epithelial cells[47]. Taken together, these data provide functional evidence of *AIRE* expression in Classical ABCs. Further work will be necessary to evaluate if *AIRE* expression in ABCs leads to self-antigen expression and productive presentation which can initiate autoimmune responses.

ABC frequency predicts neutralising antibody response to COVID-19 vaccination

To investigate the impact of ABCs on mRNA-LNP vaccination, we next analysed the immune response to the mRNA BNT162b2 COVID-19 vaccine in patients with variable expansion of ABCs, including healthy controls (HC, n=10), patients with cancer treated with ICB (ICB, n=19) and patients with *NFKB1* or *CTLA4* haploinsufficiency (IEI, n=9). One subject with phenotypic similarities to patients with CTLA4 deficiency who remained genetically unclassified was also included (**Fig. 3a** and **Supplementary Table 5**). All subjects were invited for blood sampling prior to their second vaccine dose (day 0), then at early (day 8), mid (day 21) and late (day 105) time points after this dose (**Fig. 3a**). We assessed serum samples 24h after the second dose of BNT162b2 and did not observe any difference in the levels of IL-1β, IL-12 and IFN-α between patients and controls at this time point, suggesting a similar innate immune response to the vaccine (**Supplementary Fig. 6**). Classical ABC frequencies prior to vaccination (day 0) were determined by multicolour flow cytometry staining for CD11c and CD21 (Supplementary **Fig. 7a**) and found to be elevated in patients compared with healthy controls (**Fig. 3b-c**).

Serum reactivity against SARS-CoV-2 spike (S), receptor-binding domain (RBD) and nucleocapsid (NCP) antigens was evaluated at day 21 after the second dose in the diagnostic immunology laboratory. The majority of patients (18/19 ICB, 5/8 IEI) generated IgG antibodies against S and RBD antigens (encoded by BNT162b2) at levels similar to the healthy control group (**Supplementary Fig. 7b**). These responses were unlikely to reflect previous natural infection with SARS-CoV-2, as patients did not have evidence of NCP reactivity (not encoded by BNT162b2) (**Supplementary Fig. 7b**). The quality of the SARS-CoV-2-specific antibody response can be determined by measuring the capacity of serum to neutralise authentic SARS-CoV-2 virus[48]. Overall, most subjects displayed a rapid increase

medRxiv preprint doi: https://doi.org/10.1101/2022.09.17.22280033; this version posted February 22, 2023. The copyright holder for this preprint (which was not certified by peer review) is the author/funder, who has granted medRxiv a license to display the preprint in perpetuity. All rights reserved. No reuse allowed without permission.

in neutralising antibody titres, peaking early (day 8) after their second vaccine dose (**Fig. 3d** and **Supplementary Fig. 7c**). By contrast, 5 patients (4 IEI and 1 ICB) failed to develop detectable neutralising capacity at any time point, despite having detectable anti-S antibodies. These patients are at greater risk of infection with SARS-CoV-2 and may be susceptible to prolonged or refractory COVID-19[49,50].

Critically, the frequency of pre-vaccine ABCs was inversely correlated with neutralising antibody titre at all timepoints (**Fig. 3e**), suggesting that ABCs predict both peak neutralising capacity after vaccination and the longevity of the neutralising antibody response. Indeed, at day 105, 4/8 patients with IEI and 8/16 patients treated with ICB had neutralising antibody titres which had fallen below the highest titre observed at day 0 in healthy controls, compared with 0/7 HCs (**Fig. 3d**). Individuals with neutralising capacity below this threshold showed higher frequencies of ABCs than the individuals above it (**Fig. 3f**).
A similar negative correlation between ABC frequency and neutralising capacity was still observed when we subdivided the cohort according to sex **(Supplementary Fig. 8a),** when the analysis was restricted to those subjects with ABC frequencies falling within the range observed in healthy controls **(Supplementary Fig. 8b)**, and when the analysis was restricted to those subjects with B cell frequencies falling within the range of healthy controls **(Supplementary Fig. 8c)**. Premature expansion of ABCs is therefore seen both in patients with IEI and patients with cancer treated with ICB, and (regardless of aetiology) correlates with a reduced ability to generate and maintain neutralising antibody responses to COVID-19 vaccination.

Premature expansion of ABCs is associated with lower levels of antigen-specific memory B cells

Whilst circulating antibodies derived from plasma cells wane over time, long-lived immunological memory can persist in expanded clones of antigen-specific memory B cells. We therefore assessed the frequency and differentiation of circulating SARS-CoV-2 RBD-specific B cells elicited after the second dose of vaccine using multicolour flow cytometry (**Supplementary Fig. 9a**). Strikingly, RBD-binding B cells were significantly less frequent in the different patient groups than in healthy controls (**Fig. 4a-b**). mRNA-LNP immunisation is able to induce antigen-specific ABCs[24], often termed atypical memory B cells. We therefore queried whether a high pre-vaccine ABC frequency is associated with induction of vaccine-antigen specific ABCs. Conversely, we found that the frequency of RBD-specific ABCs was reduced in all patient groups (**Supplementary Fig. 9b)**. The fraction of RBD-binding B cells amongst all $CD19^+$ B cells correlated consistently with titres of neutralising antibodies

medRxiv preprint doi: https://doi.org/10.1101/2022.09.17.22280033; this version posted February 22, 2023. The copyright holder for this preprint (which was not certified by peer review) is the author/funder, who has granted medRxiv a license to display the preprint in perpetuity. All rights reserved. No reuse allowed without permission.

(**Supplementary Fig. 9c**). In addition, RBD-specific B cell frequency immediately prior to the second vaccine dose correlated with neutralising capacity at days 8 (peak response), 21 and 105 (**Fig. 4c**). This is consistent with a causal relationship between the level of pre-existing antigen-specific B cells, and the magnitude and longevity of the neutralising antibody response upon re-encounter with the antigen. Furthermore, similar to neutralising capacity, the levels of RBD-specific B cells at later timepoints could be predicted by the frequency of ABCs at day 0 (**Fig. 4d**). Individuals with the highest frequencies of ABCs showed reduced RBD-specific B cell differentiation (**Supplementary Fig. 9c-d**).

To further analyse the cellular phenotype of rare RBD-binding B cells in a comprehensive, unbiased way, we performed unsupervised clustering and UMAP visualisation of flow cytometry data from all patients and healthy controls at all timepoints after vaccination (**Fig. 4e**). RBD-binding B cells from both patients and healthy controls were observed within clusters of memory B cells and plasmablasts (**Fig. 4f**), suggesting a quantitative reduction rather than obvious qualitative difference in the humoral response. Across all participants, the proportion of RBD-specific cells expressing plasmablast markers peaked at day 8, whilst those expressing memory B cell makers peaked a day 21 (**Fig. 4g**). Differentiation of antibody-producing cells therefore occurs contemporaneously with peak neutralising capacity (day 8). Since increased antibody production cannot be driven by the proliferation of terminally differentiated (non-dividing) plasma cells, a sizeable contribution to the neutralising antibody response after the second dose of vaccine is likely the result of this memory B cell proliferation and differentiation.

Among patients treated with ICB, we observed similar RBD-specific B cell frequencies and neutralising responses when stratified by steroidal treatment, dual/single checkpoint blockade therapy and cancer stage (III/IV) (**Supplementary Fig. 10a-b**). Conversely, we noted a reduction in both RBD specific B cell frequency and the neutralising antibody response with increasing age (**Supplementary Fig. 10c**). In theory, several factors (such as comorbidity) could impede the vaccination responses of older individuals with cancer, independent of ABC frequency. We therefore specifically examined the associations between ABC frequency, age and diminished humoral response amongst individuals under the age of 60. In this subset, RBD-specific B cell frequency and neutralising capacity were still negatively correlated with ABC frequency, but not with age (**Supplementary Fig. 10d**). These results support a primary association between pre-vaccine ABC frequency and impairment of the humoral response.

medRxiv preprint doi: https://doi.org/10.1101/2022.09.17.22280033; this version posted February 22, 2023. The copyright holder for this preprint (which was not certified by peer review) is the author/funder, who has granted medRxiv a license to display the preprint in perpetuity. All rights reserved. No reuse allowed without permission.

T cell assessment following second dose of mRNA BNT162b2 vaccination

Humoral vaccine responses require B and T lymphocyte interaction, we next assessed T cells. Circulating T follicular helper cell (Tfh) frequencies were actually increased in patients with IEI and unchanged in patients treated with ICB (**Supplementary Fig. 11a-b**). Similarly, activated ($OX40^{+}CD137^{+}$) CD4 T cell frequency was increased in patients with IEI before vaccination and this was maintained at day 21. No significant difference was observed in CD8+ T cell activation markers, nor in patients treated with ICB (**Supplementary Fig. 11c**). To assess antigen-specific responses, we next enumerated Spike-specific T cells using IFN-γ ELISpot (**Supplementary Fig. 11d**). No significant differences were observed between healthy controls and patient groups. Finally, we assessed the correlation between neutralising capacity and pre-vaccination levels of circulating Tfhs, but found no significant association. Taken together, these results suggest that the association between increased ABC frequency and diminished humoral vaccine response is independent of T cell function.

Assessment of ABCs for immune complex binding and cytokine secretion

Preclinical evidence has suggested that ABCs might impede humoral vaccine responses by diminishing affinity maturation[51]. Affinity maturation is a process requiring iterative selection of proliferating B cell clones within the germinal centre, and this takes time. However, we found substantial neutralising capacity within 8 days of vaccination, suggesting a limited requirement for substantial further affinity maturation. Furthermore, the negative correlation between ABC frequency and neutralising capacity was greatest at early time points after repeat immunisation. We therefore investigated other mechanisms by which ABCs could limit humoral vaccine responses. Further scRNAseq analysis indicated that ABCs, particularly classical ABCs, expressed high levels of the inhibitory Fc gamma receptor IIB (FcγRIIB or CD32B) (**Fig. 5a**). Expression of other Fc receptors was not observed (**Supplementary Fig. 12a**) consistent with the literature suggesting this is the only Fc receptor expressed on B lymphocytes[52]. To test this functionally, we generated immune complexes by incubation of fluorescent rabbit anti-human IgG with polyclonal human IgG at a ratio of 1:2. This resulted in complexes three times the molecular weight of rabbit IgG, consistent with a trimolecular antibody stoichiometry (**Supplementary Fig. 12b**). The binding of these complexes to B cells was Fc-dependent and significantly increased in ABCs from all patient cohorts relative to other B cell subsets (**Fig. 5b and 5d**). This positions ABCs as the B cell subset best placed to clear immune complexes directed against vaccine antigen, potentially reducing the longevity of antigen availability. Furthermore, the

medRxiv preprint doi: https://doi.org/10.1101/2022.09.17.22280033; this version posted February 22, 2023. The copyright holder for this preprint (which was not certified by peer review) is the author/funder, who has granted medRxiv a license to display the preprint in perpetuity. All rights reserved. No reuse allowed without permission.

differentiation of RBD-specific ABCs may be inhibited by signalling through the FcγRIIB limiting their contribution to memory B cell expansion or antibody secreting cell differentiation. Production of cytokines has been suggested as one mechanism by which ABCs limit B cell function[53,54] and in preclinical models of *NFKB1* deficiency B cell production of IL-6 contributes to disease pathogensis[55]. We therefore evaluated cytokine production capacity by in-vitro stimulation of B cells subsets with PMA/ionomycin and evaluated intracellular cytokines production by FACS (**Fig. 5c** and **Supplementary Fig. 12c**). This showed that although ABCs from all patient groups can produce IL-6 and TNF-α (**Fig. 5e**), the frequency of these was not higher than in other B cell subsets. Taken together within our transcriptional assessment, these results indicate ABCs from different patient groups are functionally similar and present additional mechanisms by which elevated ABCs may diminish humoral vaccine responses.

Discussion

ABC differentiation is a physiological component of the humoral response to intracellular pathogens and the vaccines that protect against them[13]. Exogenous antigen and Type I inflammatory signals trigger ABC differentiation and class switching necessary for antibody driven cell mediated cytotoxicity. Conversely, in the absence of exogenous antigen recognition and BCR signalling, TLR7 stimulation can lead to expansion of ABCs with self-reactivity[16]. In that setting ABCs may be directed against endogenous antigens, including self-antigens[16,56]. These distinct causes for ABC expansion emphasise that in any single older patient the cause for expansion (to which polygenic risk alleles, ageing, therapy, infection exposure vaccines and obesity can all contribute) is unknown. However, in young patients with ultra-rare monogenic inherited disease, expansion is caused by the specific gene disrupted. Our analysis of 4 different patient groups: healthy controls, patients with cancer treated with ICB, patients with autoimmune SLE, and patients with two distinct IEI (CTLA-4 haploinsufficiency and NFKB1 haploinsufficiency) demonstrates a homogeneity of the ABC differentiation states irrespective of the specific cause. Therefore, the pathological consequence of expanded ABCs is likely related to their increased frequency rather than an inherent difference in these cells from patients with distinct diseases. In this study we demonstrate that one of these consequences is a limitation of the humoral immune response to SARS-CoV-2 vaccination. ABCs arising from either B cell intrinsic or extrinsic reasons in preclinical models have been shown to reduce vaccine responses by impairing affinity maturation of the germinal centre response[51]. However, this mechanism alone may not account for a neutralisation difference already apparent 8 days after repeat immunisation. Our finding that ABCs express high levels of the inhibitory FcγRIIB receptor and are the B

medRxiv preprint doi: https://doi.org/10.1101/2022.09.17.22280033; this version posted February 22, 2023. The copyright holder for this preprint (which was not certified by peer review) is the author/funder, who has granted medRxiv a license to display the preprint in perpetuity. All rights reserved. No reuse allowed without permission.

cell subset best able to bind immune complexes indicates additional mechanisms by which ABCs may limit vaccine responses.

There are several limitations of this study. First, the number of people studied was modest, limiting the power to detect small differences in some comparisons and precluding a formal multivariate analysis. Second, many characteristics of ABCs may contribute to an impaired humoral vaccine response, including (but not limited to) reduced affinity maturation, signalling through inhibitory FcγRIIB and clearance of antigen. We have not quantified the extent of affinity maturation in this study, nor yet performed the detailed preclinical experiments necessary to determine the relative contribution of these mechanisms. Third, absolute numbers of ABCs were not quantified in this study, it is not possible to ascertain whether the number of ABCs or the skewing of the B cell repertoire towards this differentiation state, leads to the impairment in vaccine responses. Finally, we cannot be certain that a breach of self-tolerance has triggered the ABC expansion in patients with *NFKB1* and *CTLA4* haploinsufficiency, since this expansion could also be reactive to intracellular pathogens (to which these patients may be more susceptible).

Despite these limitations our finding that patients with increased ABC frequency have a reduced B cell vaccine response, leading to reduced neutralising capacity and reduced memory B cell formation is of immediate clinical relevance. Overall, these results place ABC frequency as a predictive biomarker for reduced vaccine protection which could guide booster vaccination schedules for patients at risk of breakthrough infection.

medRxiv preprint doi: https://doi.org/10.1101/2022.09.17.22280033; this version posted February 22, 2023. The copyright holder for this preprint (which was not certified by peer review) is the author/funder, who has granted medRxiv a license to display the preprint in perpetuity. All rights reserved. No reuse allowed without permission.

References

1 Baden, L. R. *et al.* Efficacy and Safety of the mRNA-1273 SARS-CoV-2 Vaccine. *N Engl J Med* **384**, 403-416 (2021). https://doi.org:10.1056/NEJMoa2035389

2 Polack, F. P. *et al.* Safety and Efficacy of the BNT162b2 mRNA Covid-19 Vaccine. *N Engl J Med* **383**, 2603-2615 (2020). https://doi.org:10.1056/NEJMoa2034577

3 Schmidt, A. L. *et al.* COVID-19 vaccination and breakthrough infections in patients with cancer. *Ann Oncol* **33**, 340-346 (2022). https://doi.org:10.1016/j.annonc.2021.12.006

4 Monin, L. *et al.* Safety and immunogenicity of one versus two doses of the COVID-19 vaccine BNT162b2 for patients with cancer: interim analysis of a prospective observational study. *Lancet Oncol* **22**, 765-778 (2021). https://doi.org:10.1016/S1470-2045(21)00213-8

5 Goshen-Lago, T. *et al.* Serologic Status and Toxic Effects of the SARS-CoV-2 BNT162b2 Vaccine in Patients Undergoing Treatment for Cancer. *JAMA Oncol* **7**, 1507-1513 (2021). https://doi.org:10.1001/jamaoncol.2021.2675

6 Thakkar, A. *et al.* Seroconversion rates following COVID-19 vaccination among patients with cancer. *Cancer Cell* **39**, 1081-1090 e1082 (2021). https://doi.org:10.1016/j.ccell.2021.06.002

7 Shi, J. *et al.* PD-1 Controls Follicular T Helper Cell Positioning and Function. *Immunity* **49**, 264-274 e264 (2018). https://doi.org:10.1016/j.immuni.2018.06.012

8 Wang, C. J. *et al.* CTLA-4 controls follicular helper T-cell differentiation by regulating the strength of CD28 engagement. *Proc Natl Acad Sci U S A* **112**, 524-529 (2015). https://doi.org:10.1073/pnas.1414576112

9 Khoury, D. S. *et al.* Neutralizing antibody levels are highly predictive of immune protection from symptomatic SARS-CoV-2 infection. *Nat Med* **27**, 1205-1211 (2021). https://doi.org:10.1038/s41591-021-01377-8

10 Edara, V. V. *et al.* Infection and vaccine-induced neutralizing antibody responses to the SARS-CoV-2 B.1.617.1 variant. *bioRxiv* (2021). https://doi.org:10.1101/2021.05.09.443299

11 Gilbert, P. B. *et al.* Immune correlates analysis of the mRNA-1273 COVID-19 vaccine efficacy clinical trial. *Science* **375**, 43-50 (2022). https://doi.org:10.1126/science.abm3425

12 Das, R. *et al.* Early B cell changes predict autoimmunity following combination immune checkpoint blockade. *J Clin Invest* **128**, 715-720 (2018). https://doi.org:10.1172/JCI96798

13 Cancro, M. P. Age-Associated B Cells. *Annu Rev Immunol* **38**, 315-340 (2020). https://doi.org:10.1146/annurev-immunol-092419-031130

14 Hao, Y., O'Neill, P., Naradikian, M. S., Scholz, J. L. & Cancro, M. P. A B-cell subset uniquely responsive to innate stimuli accumulates in aged mice. *Blood* **118**, 1294-1304 (2011). https://doi.org:10.1182/blood-2011-01-330530

15 Kim, C. C., Baccarella, A. M., Bayat, A., Pepper, M. & Fontana, M. F. FCRL5(+) Memory B Cells Exhibit Robust Recall Responses. *Cell Rep* **27**, 1446-1460 e1444 (2019). https://doi.org:10.1016/j.celrep.2019.04.019

16 Rubtsov, A. V. *et al.* Toll-like receptor 7 (TLR7)-driven accumulation of a novel CD11c(+) B-cell population is important for the development of autoimmunity. *Blood* **118**, 1305-1315 (2011). https://doi.org:10.1182/blood-2011-01-331462

medRxiv preprint doi: https://doi.org/10.1101/2022.09.17.22280033; this version posted February 22, 2023. The copyright holder for this preprint (which was not certified by peer review) is the author/funder, who has granted medRxiv a license to display the preprint in perpetuity. All rights reserved. No reuse allowed without permission.

17 Stewart, A. *et al.* Single-Cell Transcriptomic Analyses Define Distinct Peripheral B Cell Subsets and Discrete Development Pathways. *Front Immunol* **12**, 602539 (2021). https://doi.org:10.3389/fimmu.2021.602539

18 Rakhmanov, M. *et al.* Circulating CD21low B cells in common variable immunodeficiency resemble tissue homing, innate-like B cells. *Proc Natl Acad Sci U S A* **106**, 13451-13456 (2009). https://doi.org:10.1073/pnas.0901984106

19 Warnatz, K. *et al.* Expansion of CD19(hi)CD21(lo/neg) B cells in common variable immunodeficiency (CVID) patients with autoimmune cytopenia. *Immunobiology* **206**, 502-513 (2002). https://doi.org:10.1078/0171-2985-00198

20 Wehr, C. *et al.* A new CD21low B cell population in the peripheral blood of patients with SLE. *Clin Immunol* **113**, 161-171 (2004). https://doi.org:10.1016/j.clim.2004.05.010

21 Myles, A., Sanz, I. & Cancro, M. P. T-bet(+) B cells: A common denominator in protective and autoreactive antibody responses? *Curr Opin Immunol* **57**, 40-45 (2019). https://doi.org:10.1016/j.coi.2019.01.002

22 Rubtsov, A. V., Marrack, P. & Rubtsova, K. T-bet expressing B cells - Novel target for autoimmune therapies? *Cell Immunol* **321**, 35-39 (2017). https://doi.org:10.1016/j.cellimm.2017.04.011

23 Pape, K. A. *et al.* High-affinity memory B cells induced by SARS-CoV-2 infection produce more plasmablasts and atypical memory B cells than those primed by mRNA vaccines. *Cell Rep* **37**, 109823 (2021). https://doi.org:10.1016/j.celrep.2021.109823

24 Johnson, J. L. *et al.* The Transcription Factor T-bet Resolves Memory B Cell Subsets with Distinct Tissue Distributions and Antibody Specificities in Mice and Humans. *Immunity* **52**, 842-855 e846 (2020). https://doi.org:10.1016/j.immuni.2020.03.020

25 Rubtsov, A. V. *et al.* CD11c-Expressing B Cells Are Located at the T Cell/B Cell Border in Spleen and Are Potent APCs. *J Immunol* **195**, 71-79 (2015). https://doi.org:10.4049/jimmunol.1500055

26 Gamez-Diaz, L. *et al.* The extended phenotype of LPS-responsive beige-like anchor protein (LRBA) deficiency. *J Allergy Clin Immunol* **137**, 223-230 (2016). https://doi.org:10.1016/j.jaci.2015.09.025

27 Kuehn, H. S. *et al.* Immune dysregulation in human subjects with heterozygous germline mutations in CTLA4. *Science* **345**, 1623-1627 (2014). https://doi.org:10.1126/science.1255904

28 Schwab, C. *et al.* Phenotype, penetrance, and treatment of 133 cytotoxic T-lymphocyte antigen 4-insufficient subjects. *J Allergy Clin Immunol* **142**, 1932-1946 (2018). https://doi.org:10.1016/j.jaci.2018.02.055

29 Tuijnenburg, P. *et al.* Loss-of-function nuclear factor kappaB subunit 1 (NFKB1) variants are the most common monogenic cause of common variable immunodeficiency in Europeans. *J Allergy Clin Immunol* **142**, 1285-1296 (2018). https://doi.org:10.1016/j.jaci.2018.01.039

30 Keller, B. *et al.* The expansion of human T-bet(high)CD21(low) B cells is T cell dependent. *Sci Immunol* **6**, eabh0891 (2021). https://doi.org:10.1126/sciimmunol.abh0891

31 Schubert, D. *et al.* Autosomal dominant immune dysregulation syndrome in humans with CTLA4 mutations. *Nat Med* **20**, 1410-1416 (2014). https://doi.org:10.1038/nm.3746

32 Haslam, A., Gill, J. & Prasad, V. Estimation of the Percentage of US Patients With Cancer Who Are Eligible for Immune Checkpoint Inhibitor Drugs. *JAMA Netw Open* **3**, e200423 (2020). https://doi.org:10.1001/jamanetworkopen.2020.0423

medRxiv preprint doi: https://doi.org/10.1101/2022.09.17.22280033; this version posted February 22, 2023. The copyright holder for this preprint (which was not certified by peer review) is the author/funder, who has granted medRxiv a license to display the preprint in perpetuity. All rights reserved. No reuse allowed without permission.

33 Bhamidipati, K. *et al.* CD52 Is Elevated on B cells of SLE Patients and Regulates B Cell Function. *Front Immunol* **11**, 626820 (2020). https://doi.org:10.3389/fimmu.2020.626820

34 Rincon-Arevalo, H. *et al.* Deep Phenotyping of CD11c(+) B Cells in Systemic Autoimmunity and Controls. *Front Immunol* **12**, 635615 (2021). https://doi.org:10.3389/fimmu.2021.635615

35 Isnardi, I. *et al.* Complement receptor 2/CD21- human naive B cells contain mostly autoreactive unresponsive clones. *Blood* **115**, 5026-5036 (2010). https://doi.org:10.1182/blood-2009-09-243071

36 Terrier, B. *et al.* Expansion of functionally anergic CD21-/low marginal zone-like B cell clones in hepatitis C virus infection-related autoimmunity. *J Immunol* **187**, 6550-6563 (2011). https://doi.org:10.4049/jimmunol.1102022

37 Bashford-Rogers, R. J. *et al.* Network properties derived from deep sequencing of human B-cell receptor repertoires delineate B-cell populations. *Genome Res* **23**, 1874-1884 (2013). https://doi.org:10.1101/gr.154815.113

38 Stephenson, E. *et al.* Single-cell multi-omics analysis of the immune response in COVID-19. *Nat Med* **27**, 904-916 (2021). https://doi.org:10.1038/s41591-021-01329-2

39 Suo, C. *et al.* Dandelion utilizes single cell adaptive immune receptor repertoire to explore lymphocyte developmental origin. *bioRxiv* (2023). https://doi.org:10.1101/2022.11.18.517068

40 Gies, V. *et al.* B cells differentiate in human thymus and express AIRE. *J Allergy Clin Immunol* **139**, 1049-1052 e1012 (2017). https://doi.org:10.1016/j.jaci.2016.09.044

41 Yamano, T. *et al.* Thymic B Cells Are Licensed to Present Self Antigens for Central T Cell Tolerance Induction. *Immunity* **42**, 1048-1061 (2015). https://doi.org:10.1016/j.immuni.2015.05.013

42 Hubert, F. X. *et al.* A specific anti-Aire antibody reveals aire expression is restricted to medullary thymic epithelial cells and not expressed in periphery. *J Immunol* **180**, 3824-3832 (2008). https://doi.org:10.4049/jimmunol.180.6.3824

43 Mathis, D. & Benoist, C. Aire. *Annu Rev Immunol* **27**, 287-312 (2009). https://doi.org:10.1146/annurev.immunol.25.022106.141532

44 Fergusson, J. R. *et al.* Maturing Human CD127+ CCR7+ PDL1+ Dendritic Cells Express AIRE in the Absence of Tissue Restricted Antigens. *Front Immunol* **9**, 2902 (2018). https://doi.org:10.3389/fimmu.2018.02902

45 Rubtsova, K. *et al.* B cells expressing the transcription factor T-bet drive lupus-like autoimmunity. *J Clin Invest* **127**, 1392-1404 (2017). https://doi.org:10.1172/JCI91250

46 Phalke, S. *et al.* Molecular mechanisms controlling age-associated B cells in autoimmunity. *Immunol Rev* **307**, 79-100 (2022). https://doi.org:10.1111/imr.13068

47 Melo-Lima, B. L. *et al.* The Autoimmune Regulator (Aire) transactivates HLA-G gene expression in thymic epithelial cells. *Immunology* **158**, 121-135 (2019). https://doi.org:10.1111/imm.13099

48 Gerber, P. P. *et al.* A protease-activatable luminescent biosensor and reporter cell line for authentic SARS-CoV-2 infection. *PLoS Pathog* **18**, e1010265 (2022). https://doi.org:10.1371/journal.ppat.1010265

49 Baang, J. H. *et al.* Prolonged Severe Acute Respiratory Syndrome Coronavirus 2 Replication in an Immunocompromised Patient. *J Infect Dis* **223**, 23-27 (2021). https://doi.org:10.1093/infdis/jiaa666

medRxiv preprint doi: https://doi.org/10.1101/2022.09.17.22280033; this version posted February 22, 2023. The copyright holder for this preprint (which was not certified by peer review) is the author/funder, who has granted medRxiv a license to display the preprint in perpetuity. All rights reserved. No reuse allowed without permission.

50 Buckland, M. S. *et al.* Treatment of COVID-19 with remdesivir in the absence of humoral immunity: a case report. *Nat Commun* **11**, 6385 (2020). https://doi.org:10.1038/s41467-020-19761-2

51 Zhang, W. *et al.* Excessive CD11c(+)Tbet(+) B cells promote aberrant TFH differentiation and affinity-based germinal center selection in lupus. *Proc Natl Acad Sci U S A* **116**, 18550-18560 (2019). https://doi.org:10.1073/pnas.1901340116

52 Pritchard, N. R. & Smith, K. G. B cell inhibitory receptors and autoimmunity. *Immunology* **108**, 263-273 (2003). https://doi.org:10.1046/j.1365-2567.2003.01592.x

53 Ratliff, M., Alter, S., Frasca, D., Blomberg, B. B. & Riley, R. L. In senescence, age-associated B cells secrete TNFalpha and inhibit survival of B-cell precursors. *Aging Cell* **12**, 303-311 (2013). https://doi.org:10.1111/acel.12055

54 Riley, R. L., Khomtchouk, K. & Blomberg, B. B. Age-associated B cells (ABC) inhibit B lymphopoiesis and alter antibody repertoires in old age. *Cell Immunol* **321**, 61-67 (2017). https://doi.org:10.1016/j.cellimm.2017.04.008

55 de Valle, E. *et al.* NFkappaB1 is essential to prevent the development of multiorgan autoimmunity by limiting IL-6 production in follicular B cells. *J Exp Med* **213**, 621-641 (2016). https://doi.org:10.1084/jem.20151182

56 Rubtsov, A. V., Rubtsova, K., Kappler, J. W. & Marrack, P. TLR7 drives accumulation of ABCs and autoantibody production in autoimmune-prone mice. *Immunol Res* **55**, 210-216 (2013). https://doi.org:10.1007/s12026-012-8365-8

medRxiv preprint doi: https://doi.org/10.1101/2022.09.17.22280033; this version posted February 22, 2023. The copyright holder for this preprint (which was not certified by peer review) is the author/funder, who has granted medRxiv a license to display the preprint in perpetuity. All rights reserved. No reuse allowed without permission.

Figure Legends

Figure 1. Single cell transcriptional signature of ABCs. Magnetically enriched B cells from PBMCs were analysed through droplet-based single cell RNA sequencing technology (n = 52402). **a-c.** UMAPs of cells from all individuals coloured by (**a)** annotated Louvain clusters, (**b)** health condition (HC, healthy controls; ICB, immune-checkpoint blockade treated cancer patients; IEI CTLA-4/NFKB1, inborn errors of immunity, CTLA-4 and NFKB1 mutants respectively; SLE, systemic lupus erythematosus patients), and (**c**) gender. Dots represent a single cell. **d.** Proportion of total cells from each health condition belonging to each cluster, clusters coloured as indicated. **e.** Expression of 46 genes in each B cell cluster which define the different subpopulations. Dot size represents proportion of cells within a cluster expressing the indicated gene and colours represent the average expression level. **f.** Heatmap representing scaled expression values of genes associated with antigen uptake, processing and class-II presentation in each cluster. **g.** Gene ontology enrichment analysis of biological processes associated with upregulated genes in classical ABCs. GO terms with highest fold enrichments are ranked by -log (P value). Dot size is proportional to the fold enrichment.

Figure 2. Classical ABC expression of AIRE and AIRE target genes. a. Volcano plot displaying the differentially expressed genes in ABCs compared to other B cell clusters. Upregulated genes associated with antigen uptake, processing and MHC class II presentation are labelled. AIRE gene is coloured in green. **b.** UMAP of all B cells coloured by kernel density estimation of AIRE expression level across all identified B cell subsets. UMAP showing the different B cell clusters inset. **c.** Percentage of cells which are $AIRE^+$ in each cluster. **d.** Violin plot comparing expression score of tissue restricted antigens (gene set from Yamano *et al*) in AIRE expressing cells and all other cells. Statistical testing via Wilcoxon rank sum test.

Figure 3. Correlation between frequency of ABCs and neutralising antibody response to COVID-19 vaccination. a. Cohort details. Samples were collected at days 0, 8, 21 and 105 after the 2nd dose of BNT162b2 vaccine (healthy controls (HC), grey; patients with rare inborn errors of immunity (IEI): NFKB1 red, CTLA-4 and unclassified orange; patients treated with ICB, blue). **b**. Representative FACS contour plots of $CD21^{lo}CD11c^+$ ABCs in CD19 B cells. **c.** Frequencies of B cells within total lymphocytes and frequencies ABCs within total B cells, at day 0. **d.** Neutralising antibody titres at 50% inhibition (NT_{50}) against wildtype SARS-CoV-2 at indicated timepoints after 2nd vaccine dose. The limit of detection of

medRxiv preprint doi: https://doi.org/10.1101/2022.09.17.22280033; this version posted February 22, 2023. The copyright holder for this preprint (which was not certified by peer review) is the author/funder, who has granted medRxiv a license to display the preprint in perpetuity. All rights reserved. No reuse allowed without permission.

the assay is indicated (grey dotted line at NT_{50} = 20), and an arbitrary threshold at the highest NT_{50} from the HC group at day 0 (brown dashed line). **e**. Correlations between frequencies of ABCs amongst B cells at day 0 and NT_{50}s at days 8, 21 and 105. **f.** Frequencies of ABCs amongst $CD19^+$ B cells for individuals above and below the arbitrary threshold indicated in panel **d** at day 105. Where specified, differences between groups were determined using two-tailed non-parametric Mann Whitney tests. Spearman's rank correlation coefficients (rho) are shown, together with indicative linear regression lines plus, **c-f** each point represents one individual.

Figure 4. Correlation between frequency of RBD-specific B cells and neutralising antibody response to COVID-19 vaccination. a. Representative flow cytometry plots displaying RBD-specific B cell populations amongst total $CD19^+$ B cells for different study groups 0, 8, 21 and 105 days (D0, D8, D21 and D105) after the second dose of BNT162b2 vaccine. **b.** Frequencies of RBD-specific B cells amongst all $CD19^+$ B cells in HC, IEI and ICB patients at days 0, 8, 21 and 105. Each dot represents a single individual (healthy controls (HC), grey; patients with rare inborn errors of immunity (IEI): (NFKB1) red, (CTLA-4 and unclassified) orange; patients treated with ICB, blue). Two-way ANOVA with Tukey's multiple comparisons test for statistical analysis. **c.** Correlations between frequencies of RBD-specific B cells amongst all CD19+ B cells at day 0 and NT_{50}s at days 8, 21 and 105. **d.** Correlations between frequencies of ABCs amongst B cells at day 0 and frequencies of RBD-specific B cells at days 8, 21 and 105. **e.** UMAP projection of total B cells from all donors at all time points displaying memory B cell (MBCs, purple) and plasmablast (PBs, green) populations. **f.** RBD-specific B cells with MBC (purple) or PB (green) phenotype are shown at days 0, 8, 21 and 105 (columns) for HC (top), IEI (middle) and ICB (bottom) groups. **g.** Kinetics of RBD-binding cell frequencies amongst MBCs or PBs. Samples with no detectable levels of RBD-specific cells are plotted at an arbitrary value of 10^{-4} in (B) and 10^{-3} in (G). Where specified, statistical significance between groups was determined using one-way ANOVA (G). Spearman's rank correlation coefficients (rho) are shown, together with indicative linear regression lines where appropriate.

Figure 5. ABCs express higher levels of Fc γ receptor IIB and bind higher proportions of immune complexes than other B cells subsets. a. Violin plots displaying the expression levels of *FCGR2B* on different B cell subsets. **b.** Representative flow cytometry contour plots displaying immune complex binding (contour plots in green) with or without a previous incubation with Fc block by age-associated B cells (ABCs), memory B cells (MBCs), naïve B cells and plasmablasts (PBs). **c.** Representative flow cytometry contour

medRxiv preprint doi: https://doi.org/10.1101/2022.09.17.22280033; this version posted February 22, 2023. The copyright holder for this preprint (which was not certified by peer review) is the author/funder, who has granted medRxiv a license to display the preprint in perpetuity. All rights reserved. No reuse allowed without permission.

plots displaying cytokines production (IL-6 and TNF-α, PMA/ionomycin stimulation for 5h, 37C, brefeldin A) by age-associated B cells (ABCs), memory B cells (MBCs), naïve B cells and plasmablasts (PBs). **d.** Frequencies of ICs binding cells in different B cell subsets. **e**. Frequencies of cells with IL-6- and TNF-α-secreting capacity in different B cell subsets. Where specified, statistical significance between groups was determined using one-way ANOVA.

Supplemental Figures and Tables

Supplementary Figure 1. Single cell assessment of B cells from different patients. a. Magnetically enriched B cells from PBMCs were labelled using barcode featuring and analysed through droplet-based single cell RNA sequencing technology. Expression of surface protein CD11c against CD21 in all B cells. **b.** Violin plots of CD21 and CD11c surface protein expression in ABCs versus other B cells with CLR-normalised expression values. Statistical testing via Wilcoxon rank sum test with Bonferroni correction. **c.** B cell clusters, with percentages of cells from healthy controls and patients coloured. **d.** UMAPs of total B cells per health condition coloured by annotated clusters (HC, healthy controls; ICB, immune-checkpoint blockade treated patients; IEI CTLA-4/NFKB1, immune errors of immunity, CTLA-4 and NFKB1 mutants respectively; SLE, systemic lupus erythematosus patients). **e.** Number of samples from each gender, coloured as indicated, in healthy controls and patients (Left). B cell clusters, with percentages of cells from each gender coloured (Right). **f.** Healthy controls and patients, with percentages of cells from each cluster coloured as indicated, divided into two groups based on sex. Dots represent a single cell (a-b and d).

Supplementary Figure 2. Class-I related genes expression within the different B cell clusters. Heatmap representing scaled expression values of genes associated with antigen uptake, processing and class-I presentation in each cluster.

Supplementary Figure 3. Clonal expansion and clonal relationships of different B cell subsets. Dot plot of Gini index against Degree index.

Supplementary Figure 4. Classical age-associated B cells upregulate AIRE in different health conditions. a. UMAP of total B cells showing AIRE+ cells coloured by density of expression. **b.** UMAPs of total B cells per health condition coloured by kernel density estimation of AIRE expression level (HC, healthy controls; ICB, immune-checkpoint

medRxiv preprint doi: https://doi.org/10.1101/2022.09.17.22280033; this version posted February 22, 2023. The copyright holder for this preprint (which was not certified by peer review) is the author/funder, who has granted medRxiv a license to display the preprint in perpetuity. All rights reserved. No reuse allowed without permission.

blockade treated patients; IEI CTLA-4/NFKB1, immune errors of immunity, CTLA-4 and NFKB1 mutants respectively; SLE, systemic lupus erythematosus patients).

Supplementary Figure 5. Expression of B cell AIRE targets in different cells/tissues. Heatmap representing scaled transcript per million (nTPM) values.

Supplementary Figure 6. Analysis of cytokine levels in serum. Summary graphs showing IL-1β, IL-12 and IFN-α concentrations (pg/ml) in serum from HC, healthy controls; ICB, immune-checkpoint blockade treated patients; and IEI, immune errors of immunity patients 24h after the second dose of BNT162b2 vaccine. Differences between groups were determined using two-tailed non-parametric Kruskal-Wallis tests.

Supplementary Figure 7. Decline of the neutralising capacity after second dose of BNT162b2 vaccine. a. Gating strategy to identify age-associated B cell (ABCs, SingletsLiveCD3-CD19+CD21-CD11+) subset from total B cell population (CD19+). **b.** IgG end-point titres specific to the spike (S), receptor-binding domain (RBD) and nucleocapsid (NCP) proteins of SARS-CoV2 at day 21 after the second dose of BNT162b2 vaccine. **c**. Neutralising antibody titres at 50% inhibition (NT_{50}) against wildtype SARS-CoV-2 at indicated timepoints after 2nd dose of BNT162b2 vaccine (healthy controls (HC), grey; patients with rare inborn errors of immunity (IEI): (NFKB1) red, (CTLA-4 and unclassified) orange; patients treated with ICB, blue). The limit of detection of the assays is shown (grey dotted line at NT_{50} = 20). Where specified, statistical significance between groups was determined using 2-way ANOVA with Tukey's multiple comparisons test.

Supplementary Figure 8. Correlations of ABC frequency and neutralising capacity. a. Spearman's correlations of ABC frequency at day 0 and NT_{50} at days 8, 21 and 105 in males and females. **b.** Spearman's correlations of ABC frequency at day 0 and NT_{50} at days 8, 21 and 105 in the subset of the cohort which had an ABC frequency within the range of healthy controls. **c.** Spearman's correlations of ABC frequency at day 0 and NT_{50} at days 8, 21 and 105 in the subset of the cohort which had a B lymnphocyte frequency within the range of healthy controls. Spearman's rank correlation coefficients (rho) are shown, together with indicative linear regression lines where appropriate.

Supplementary Figure 9. ABC expansion is associated with impaired humoral responses to COVID-19 vaccination. a. Gating strategy to identify RBD-specific B cell (SingletsLiveStreptavidinBV711-CD19+RBDAF488+RBDAF647+) subset after the second

medRxiv preprint doi: https://doi.org/10.1101/2022.09.17.22280033; this version posted February 22, 2023. The copyright holder for this preprint (which was not certified by peer review) is the author/funder, who has granted medRxiv a license to display the preprint in perpetuity. All rights reserved. No reuse allowed without permission.

dose of BNT162b2 vaccine. **b.** Frequencies of RBD-specific ABCs amongst all ABCs ($CD21^{lo}CD11c^{+}CD19^{+}$ B cells) in healthy controls and patients at days 0, 8, 21 and 105. Each dot represents a single individual (healthy controls (HC), grey; patients with rare inborn errors of immunity (IEI): (NFKB1) red, (CTLA-4 and unclassified) orange; patients treated with ICB, blue). Two-way ANOVA with Tukey's multiple comparisons test for statistical analysis of RBD-binding B cells amongst groups. P values are indicated. **c.** Multiple variable dot plots showing Spearman correlations between RBD-specific B cells and NT_{50} at days 8, 21 and 105 after the second dose of BNT162b2 vaccine. Dot size represents ABC frequency per individual. Colours indicate healthy controls and patients. **d.** Correlation matrix using Spearman's rank correlation amongst ABC and B cell frequencies at day 0; and RBD frequencies and NT_{50} values at days 0, 8, 21 and 105 for the second dose of BNT162b2 vaccine. Data include all samples enrolled in the study; Rho values are shown per correlation.

Supplementary Figure 10. Humoral response analysis based on treatment, cancer stage and age. a. Neutralising antibody titres at 50% inhibition (NT_{50}) against wildtype SARS-CoV-2 (top) and frequencies of RBD-specific B cells amongst all $CD19^{+}$ B cells (bottom) at day 21 after 2nd vaccine dose in cancer patients grouped by steroidal drugs treatment and ICB therapy. **b.** Neutralising antibody titres at 50% inhibition (NT_{50}) against wildtype SARS-CoV-2 (top) and frequencies of RBD-specific B cells amongst all $CD19^{+}$ B cells (bottom) at day 21 after 2nd vaccine dose in cancer patients grouped by cancer stage. Each dot represents a single individual (healthy controls (HC), grey; patients treated with ICB, blue). **c.** Spearman's correlations between NT_{50}s (top) or frequencies of RBD-specific B cells amongst all $CD19^{+}$ B cells (bottom) at day 21 and age of all individuals. **d.** Spearman's correlations of ABC frequency at day 0 (left) and NT_{50}s (top) or frequencies of RBD-specific B cells amongst all $CD19^{+}$ B cells (bottom) at day 21 in individuals under the age of 60. Spearman's correlations of age of individuals under 60's (right) and NT_{50}s (top) or frequencies of RBD-specific B cells amongst all $CD19^{+}$ B cells (bottom) at day 21. Spearman's rank correlation coefficients (rho) are shown, together with indicative linear regression lines where appropriate. Each dot represents a single individual (healthy controls (HC), grey; patients with rare inborn errors of immunity (IEI): (NFKB1) red, (CTLA-4 and unclassified) orange; patients treated with ICB, blue).

Supplementary Figure 11. T cell assessment. a. Gating strategy to identify T follicular helper cells (Tfhs, SingletsLiveCD3+CD8-CD4+CD45RA-PD-1+CXCR5+) subset. **b.** Frequencies of Tfhs amongst CD4+CD45RO+(CD45RA-) T cells in healthy controls and

medRxiv preprint doi: https://doi.org/10.1101/2022.09.17.22280033; this version posted February 22, 2023. The copyright holder for this preprint (which was not certified by peer review) is the author/funder, who has granted medRxiv a license to display the preprint in perpetuity. All rights reserved. No reuse allowed without permission.

patients at days 0 and 21 after the second BNT162b2 dose. **c.** Frequencies of OX40 and CD137 expression on CD4+ and CD8+ T cells amongst total CD4+ or CD8+ T cells, respectively, in healthy controls and patients at days 0 and 21 after the second BNT162b2 dose. **d.** Spike-specific T cell responses quantified by Elispot. SFU = Interferon gamma spot forming units. **e.** Spearman's correlation between Tfh frequency at day 0 and NT_{50} at days 8, 21 and 105 post-second dose vaccination. Spearman's rank correlation coefficients (rho) are shown, together with indicative linear regression lines where appropriate. Each dot represents a single individual (healthy controls (HC), grey; patients with rare inborn errors of immunity (IEI): (NFKB1) red, (CTLA-4 and unclassified) orange; patients treated with ICB, blue). One-way ANOVA (d) or Two-way ANOVA with Tukey's multiple comparisons test (b-c) for statistical analysis. P values are indicated.

Supplementary Figure 12. Fc γ receptor expression on B cells. a. Violin plots displaying the expression levels of FCGR3A, FCGR2A and FCGR1A on different B cell subsets. **b.** Relative size of detection antibody (Ab-AF647) or immune complexes (Hu Igs – Ab-AF647) by means of hydrodynamic radius (R_h) measured by Microfluidic Diffusional Sizing (MDS). **c.** Representative flow cytometry contour plots displaying cytokines production (IL-6 and TNF-α) by age-associated B cells (ABCs), memory B cells (MBCs), naïve B cells and plasmablasts (PBs) on unstimulated cells incubated for 5h at 37C with brefeldin A.

Supplementary Table 1 – Differentially expressed genes related to Figure 1e

Supplementary Table 2 – Top 20 biological processes from the gene ontology enrichment analysis

Supplementary Table 3 – Differentially expressed genes related to Figure 2a

Supplementary Table 4 – AIRE target genes related to Fig. 2d and Supp. Fig. 5

Supplementary Table 5 – Characteristics of Inborn Errors of Immunity (IEI) patients and Immune Checkpoint blockade treated (ICB) patients

Supplementary Table 6 – Flow cytometry antibodies details

Acknowledgements

This work was funded by the MRC (grant ref. MC_UU_00025/12), the Medical Research Foundation (MRF-057-0002-RG-THAV-C0798) and The Evelyn Trust (grant number 20/40). NJM was supported by the MRC (CSF ref. MR/P008801/1 to NJM), NHSBT (grant ref. WPA15-02 to NJM) and Addenbrooke's Charitable Trust (grant ref. 900239 to NJM). KW has received funding by the Deutsche Forschungsgemeinschaft (WA 1597/6-1 and WA 1597/7-1). The authors thank the Flow Cytometry Services provided by Lucia Pereira Giraldez at the

medRxiv preprint doi: https://doi.org/10.1101/2022.09.17.22280033; this version posted February 22, 2023. The copyright holder for this preprint (which was not certified by peer review) is the author/funder, who has granted medRxiv a license to display the preprint in perpetuity. All rights reserved. No reuse allowed without permission.

MRC-Toxicology Unit, University of Cambridge and Katarzyna Kania from CRUK-CI-Genomics for advice on single cell RNA sequencing experiments.

Competing interest

The authors declare no competing financial interests.

Corresponding Authors

Correspondence and requests for materials should be addressed to James Thaventhiran (jedt2@cam.ac.uk) and Juan Carlos Yam-Puc (jcy28@cam.ac.uk).

medRxiv preprint doi: https://doi.org/10.1101/2022.09.17.22280033; this version posted February 22, 2023. The copyright holder for this preprint (which was not certified by peer review) is the author/funder, who has granted medRxiv a license to display the preprint in perpetuity. All rights reserved. No reuse allowed without permission.

Methods

Patient recruitment and ethics

Enrolment of patients into this study was based on the deficiency of particular genes of interest (IEI: CTLA4, LRBA, NFkB1, NFkB2) or clinical diagnostics (ICB, n = 19), whilst healthy controls for this study were enrolled based on their clinical healthy status (n = 10). Sample-size calculation was limited due to IEI patients in the study (n = 9) reflect a rare population of individuals within the general population that we were able to recruit (Supplementary Table 5).

The research was conducted in accordance with the principles of Good Clinical Practice and following approved protocols of the NIHR National Bioresource. Samples were collected with the written informed consent of all study participants under the NIHR National BioResource - Research Tissue Bank (NBR-RTB) ethics (REC:17/EE/0025) or under the Barts and the London Immunology Registry (REC: 11/LO/1689). Clinical data were collected by Clinical Immunology Consultants at Cambridge University Hospital and Bart's Health via the Electronic Healthcare Record (Epic), or direct patient contact.

The patients and healthy controls were consented under the East of England Cambridge South national research ethics committee (REC) reference 13/EE/0325 or Barts and the London Immunology Registry (REC: 11/LO/1689).

Blood donation and separation

Patients and controls gave voluntary blood samples prior to second dose and at early (day 8), mid (day 21) and late (day 105) timepoints following their second BNT162b2 vaccine. Where sample size of individual assays was not the same as the total sample size, this was because there was no sample collection at those specific time points. Samples may have also been excluded if there was serological evidence of prior exposure to SARS-COV-2. Peripheral blood samples were acquired in either lithium heparin or serum separating tubes. Peripheral blood mononuclear cells (PBMCs) were isolated by a density gradient centrifugation protocol and stored at -80°C for up to a week before being transferred to liquid nitrogen until use. Whilst serum tubes were centrifuged to separate serum from cell pellet before being aliquoted and stored at -80°C until use.

Single cell library preparation and sequencing

Frozen PBMCs were thawed and B cell population was enriched using magnetic separation (Miltenyi 130-101-638). Samples were next labelled with oligonucleotide-tagged antibodies against CD11c, CD21, CD27 and CD85j (TotalSeq, BioLegend). After labelled, cell counts were adjusted to 1,035 cells per microlitre before being loaded onto a Chromium Next GEM

medRxiv preprint doi: https://doi.org/10.1101/2022.09.17.22280033; this version posted February 22, 2023. The copyright holder for this preprint (which was not certified by peer review) is the author/funder, who has granted medRxiv a license to display the preprint in perpetuity. All rights reserved. No reuse allowed without permission.

chip K (10X Genomics, 2000182) for the subsequent 5' Gene Expression and V(D)J libraries' construction according to Single cell 5' v2 protocol (CG000330 RevA, 10X Genomics). The library was quality controlled by Agilent 4150 TapeStation and quantified by RT-PCR using the KAPA library quantification kit for Illumina platforms (Roche, KK4824). Samples were sequenced on an Illumina NovaSeq with a sequencing depth of at least 50, 000 reads per cell.

Software versions

Single cell transcriptome and VDJ data was analysed using Cell Ranger software version 6.1.1 and 7.0.1 respectively, citeseq version 1.5.0, R version 4.0.3 and R packages (Seurat 4.1.0, SeuratObject 4.0.4, Scuttle 1.0.4, rstatix 0.7.0, tidyverse 1.3.0 and dplyr 1.0.8) and python packages (dandelion 0.3.0, pandas 1.1.3, numpy 1.19.2, networkx 2.5, scipy 1.5.2, blast 2.11.0, igblast 1.17.1, anndata 0.7.6, scanpy 1.7.2, changeo 1.0.2 and airr 1.3.1). Flow cytometry data and antibody titres were analysed using FlowJo 10.7.1 and GraphPad Prism 9.1.2 (225), respectively. Figures were produced using ggplot2 3.3.5, gridExtra 2.3, ComplexHeatmap 2.6.2, Nebulosa 1.0.2, RColorBrewer 1.1-2, ggrepel 0.9.1, ggpubr 0.4.0, scales 1.1.1, showtext 0.9-5 in R and GraphPad Prism 9.1.2 (225) and FlowJo 10.7.1.

Preprocessing of scRNA-seq transcriptome data

Raw FASTQ files of the gene expression library were analysed using 10x Genomics Cell Ranger software v.6.1.1 [1] and aligned to the GRCh38 genome provided by Cell Ranger. All Ig V, D, J and constant genes as well as TCR genes were deleted from the dataset so that downstream analysis is not affected by highly variable clonotype genes. For the quantification of antibody derived tags (ADT) and oligo hashtags, citeseq pipeline v.1.5.0 [2] was used. The generated hashtag count matrices as well as raw gene expression count matrices were then used as inputs for the Seurat package v.4.1.0 [3] in R v.4.0.3. Seurat objects were created from the corresponding transcript count matrices. ADT assays were added using CreateAssayObject function of Seurat to include expression levels of surface proteins. Samples were then demultiplexed using HTODemux function. Doublets and cells with no assigned hashtag were removed from objects for further analysis. Scuttle package v.1.0.4 [4] was used for quality control. 3 x Median absolute deviation (MAD) was considered as the threshold for quality control; number of features and number of read counts were filtered from both sides, whereas percentage of mitochondrial genes was filtered from upper side. The samples were log-normalized for further differential expression analysis. Before integrating all objects, they were normalized based on regularized negative binomial regression using the SCTransform function of the Seurat package, regressing out for cell

medRxiv preprint doi: https://doi.org/10.1101/2022.09.17.22280033; this version posted February 22, 2023. The copyright holder for this preprint (which was not certified by peer review) is the author/funder, who has granted medRxiv a license to display the preprint in perpetuity. All rights reserved. No reuse allowed without permission.

cycle scores, number of counts and percentage of mitochondrial genes. The objects were then integrated using the integration protocol of the Seurat package to perform batch effect correction. The objects used for integration include: four groups of healthy controls each having two subjects (total of 26900 cells in the final dataset), one group of IEI patients (5345 cells in the final dataset) and two groups of ICB patients (total of 9751 cells in the final dataset) each having four subjects, and SLE patients with 3 subjects (10406 cells in the final dataset).

SLE data

Data of SLE patients from Bhamidipati et al [5] was downloaded from GSE163121, reprocessed and integrated with other objects using the same procedure as described above.

Clustering of data

Principal component analysis (PCA) was performed on the integrated object to reduce the dimensionality of the dataset. First, clustering was done using 30 principal components (PCs) and resolution parameter of 0.1. Clusters with a high expression of non-B cell markers were removed from the dataset. After deletion of all non-B cells, the dataset consists of 52402 cells. PCs were calculated in the new dataset and unsupervised clustering was performed using 20 PCs and resolution parameter of 1.4. Cluster markers were calculated with the default parameters of the FindMarkers function. Clusters with similar markers were manually merged. Final clusters were labelled based on the differentially expressed genes in each cluster.

Gene ontology enrichment analysis

Gene ontology [6, 7] enrichment analysis was performed via PANTHER [8] from http://www.geneontology.org using the list of significantly upregulated genes from classical ABC cluster (Average log2 fold change > 0.25 and percent expressed in each group > 0.25).

Processing of scRNA-seq VDJ data

Raw FASTQ files of the VDJ library were analysed using the 10x Genomics Cell Ranger software v7.0.1 and aligned to the VDJ GRCh38 genome provided by Cell Ranger. The Dandelion package was then used for analysis of clonal expansion in different clusters [9, 10]. Using dandelion V/D/J genes were re-annotated, heavy V gene alleles and constant region calls were re-assigned and cells with poor quality contigs were filtered [11, 12]. Clones were defined based on following criterion:

i) usage of the same V and J genes

medRxiv preprint doi: https://doi.org/10.1101/2022.09.17.22280033; this version posted February 22, 2023. The copyright holder for this preprint (which was not certified by peer review) is the author/funder, who has granted medRxiv a license to display the preprint in perpetuity. All rights reserved. No reuse allowed without permission.

ii) identical CDR3 sequence length

iii) minimum of 85% sequence similarity between CDR3 sequences based on hamming distance

Dandelion was then used for generating a tree-like network for each clone based on the similarities of the full VDJ contig sequences. Vertex/node Gini index was calculated as a measure of clonal expansion in different clusters [13]. For calculating Gini index, dandelion merges identical BCRs into one node in the BCR network and the number of merged nodes are counted. The degree index from dandelion was also calculated as a measure of how many cells are connected to an individual cell in the clonal network. Both indices can vary between 0 and 1.

Geneset Scores

A list of 74 Aire-induced genes were obtained from Yamano et al., [14] after converting mouse gene IDs to human gene IDs (Supplementary Table 4). For calculating gene set score for each cell, AddModuleScore function from Seurat package was used. Briefly, average expression of genes in each cell is calculated and is subtracted by the aggregated expression of control gene sets. For selecting control gene sets, genes are first binned. Then, for each gene, control gene sets are randomly chosen from the same expression bin as that gene, so that they have similar expression patterns to Aire target genes. To explore the expression pattern of these genes in different tissues, normalised transcript per million (nTPM) values were extracted in different immune cells and different tissues from the human protein atlas website (https://v22.proteinatlas.org/download/rna_immune_cell.tsv.zip and https://v22.proteinatlas.org/download/rna_tissue_consensus.tsv.zip, respectively). In addition to two groups of B lymphocytes, those tissues and cells that have maximum expression of at least one of the genes from our list were kept.

Kernel density estimation of gene expression

Nebulosa package v 1.0.2 [15] was used for calculating and plotting gene-weighted density estimation of AIRE expression.

SARS-CoV-2 serology

A Luminex bead-based immunoassay was used to quantify specific antibodies to full-length trimeric spike (S), spike receptor binding domain (RBD) and nucleocapsid (NCP) of SARS-CoV-2 as previously described [16, 17]. Briefly, a multiplex assay was established by covalently coupling recombinant SARS-CoV-2 proteins to distinct carboxylated bead sets (Luminex, Netherlands). The S protein used here was the S-R/PP described in Xiong et al

medRxiv preprint doi: https://doi.org/10.1101/2022.09.17.22280033; this version posted February 22, 2023. The copyright holder for this preprint (which was not certified by peer review) is the author/funder, who has granted medRxiv a license to display the preprint in perpetuity. All rights reserved. No reuse allowed without permission.

[16], and the RBD protein was described by Stadlbauer et al [18]. The NCP protein used is a truncated construct of the SARS-CoV-2 NCP protein comprising residues 48–365 (both ordered domains with the native linker) with an N terminal uncleavable hexahistidine tag. NCP was expressed in E. Coli using autoinducing media for 7h at 37°C and purified using immobilised metal affinity chromatography (IMAC), size exclusion and heparin chromatography. The S-, RBD- and NCP-coupled bead sets were incubated with patient sera at 3 dilutions (1/100, 1/1000, 1/10000) for 1 h in 96-well filter plates (MultiScreen HTS; Millipore) at room temperature in the dark on a horizontal shaker. After washes, beads were incubated for 30 min with a PE-labeled anti–human IgG-Fc antibody (Leinco/Biotrend), washed as described above, and resuspended in 100 µl PBS/ Tween. Antibody-specific binding was interpreted using Exponent Software V31 software on the Luminex analyzer (Luminex / R&D Systems) and reported as mean fluorescence intensity (MFI). The diagnostic thresholds used adhered to UK national guidelines.

Neutralising antibodies to SARS-CoV-2

The SARS-CoV-2 used in this study was a wildtype (lineage B) virus (SARS-CoV-2/human/Liverpool/REMRQ0001/2020), a kind gift from Ian Goodfellow (University of Cambridge), isolated early in the COVID-19 pandemic by Lance Turtle (University of Liverpool) and David Matthews and Andrew Davidson (University of Bristol) [19-21] from a patient on the Diamond Princess cruise ship. Sera were heat-inactivated at 56°C for 30 mins before use, and neutralising antibody titres at 50% inhibition (NT50s) measured as previously described [22, 23].

In brief, luminescent HEK293T-ACE2-30F-PLP2 reporter cells (clone B7) expressing SARS-CoV-2 Papain-like protease-activatable circularly permuted firefly luciferase (FFluc) were seeded in flat-bottomed 96-well plates. The next day, SARS-CoV-2 viral stock (MOI=0.01) was pre-incubated with a 3-fold dilution series of each serum for 2 h at 37°C, then added to the cells. 16 h post-infection, cells were lysed in Bright-Glo Luciferase Buffer (Promega) diluted 1:1 with PBS and 1% NP-40, and FFluc activity measured by luminometry. Experiments were conducted in duplicate.

To obtain NT50s, titration curves were plotted as FFluc vs log (serum dilution), then analysed by non-linear regression using the Sigmoidal, 4PL, X is log(concentration) function in GraphPad Prism. NT50s were reported when (1) at least 50% inhibition was observed at the lowest serum dilution tested (1:20), and (2) a sigmoidal curve with a good fit was generated. For purposes of visualisation and ranking, samples for which visual inspection of the titration curve indicated inhibition at low dilutions, but which did not meet criteria (1) and (2) above, were assigned an arbitrary NT50 of 4.

medRxiv preprint doi: https://doi.org/10.1101/2022.09.17.22280033; this version posted February 22, 2023. The copyright holder for this preprint (which was not certified by peer review) is the author/funder, who has granted medRxiv a license to display the preprint in perpetuity. All rights reserved. No reuse allowed without permission.

World Health Organisation International Standard 20/136 (WHO IS 20/136) has an NT50 of 1967 against wildtype SARS-CoV-2 when measured in this assay. This standard comprises pooled convalescent plasma obtained from 11 individuals which, when reconstituted, is assigned an arbitrary neutralising capacity of 1000 IU/ml against early 2020 SARS-CoV-2 isolates [24]. NT50s from this study may therefore be converted to IU/ml using a calibration factor of 1000/1967 (0.51), with a limit of quantitation of 10.2 IU/ml (corresponding to an NT50 of 20).

Flow cytometric analysis

Frozen PBMCs were thawed and stained with B cell panel antibody cocktail (Supplementary Table 6). All samples were acquired on the BD LSRFortessa using FACSDIVA software (BD-Biosciences). FCS files were exported and analysed using FlowJo v10.7.2 (BD-Biosciences) software. Additionally, a uniform manifold approximation and projection (UMAP) algorithm for dimensional reduction was performed on a concatenated FCS file comprising events from the CD19+ gate from HC, IEI and ICB samples analysed, utilizing the UMAP FlowJo plugin (v3.1). The composite samples were gated as indicated on Supplementary Figures for RBD+ B cell identification and then overlaid by study group in the UMAP generated, for additional visualisation. XShift (v1.4.1) and ClusterExplorer (1.5.15) plugins were used for unsupervised cluster generation and exploration, respectively. Class-switched memory B cells and plasmablasts/plasma cells were selected based on the expression of CD19+IgD-IgM-CD38-CD27+ and CD19+IgD-IgM-CD38+/highCD27+/high, respectively.

RBD tetramer production

SARS-CoV-2 RBD was expressed with N-terminal fusion of His-Zbasic-TEV module (8×His tag, Zbasic domain [25] and TEV protease cleavage site) and C-terminal Avi-tag in BL21(DE3) cells (Novagen) cultured in 2xYT media at 37°C. RBD containing inclusion bodies were isolated and solubilised. The denatured protein was first purified by immobilized metal affinity chromatography using PureCube Ni-NTA resin, eluted and refolding was allowed to proceed for 72 hours at 4°C. N-terminal fusion tag was cleaved off by NHis-TEVpro (produced in-house). Biotinylation of the RBD protein was carried out using 5 mM MgCl2, 2 mM ATP, 150 µM biotin and 50 µg/ml of biotin ligase BirA-CHis (produced in-house). The excess of biotinylated RBD protein was then incubated with 0.5 mg/ml of fluorescently labelled Streptavidin (BioLegend) for 1 hour at room temperature and, finally, RBD-Streptavidin complexes were separated by size exclusion chromatography using a

medRxiv preprint doi: https://doi.org/10.1101/2022.09.17.22280033; this version posted February 22, 2023. The copyright holder for this preprint (which was not certified by peer review) is the author/funder, who has granted medRxiv a license to display the preprint in perpetuity. All rights reserved. No reuse allowed without permission.

Superdex 200 Increase 10/300 GL column (Cytiva). The RBD-Streptavidin complexes were then analysed by SDS-PAGE.

Immune complex binding assay

Immune complexes were generated by incubation of 2 µg of human immunoglobulins (Biolegend 422302) with 1 µg of Alexa Fluor 647 AffiniPure Rabbit Anti-Human IgG (Jackson ImmunoResearch 309-605-006) for 1h at room temperature and diluted 1 in 10 before cell binding. Immune complex size was analysed by means of hydrodynamic radius (R_h) measured by Microfluidic Diffusional Sizing (MDS) on a Fluidity One-W (Fluidic Analytics) instrument. Thawed PBMCs were or not incubated with Fc block for 30 minutes before interaction with ICs for 10 minutes at room temperature. After immune complex binding, PBMCs were fixed with PFA at 1% for 30 minutes and then washed. After fixation, PBMCs were stained with a B cell antibody cocktail panel for surface labelling. All samples were acquired on the BD LSRFortessa using FACSDIVA software (BD-Biosciences). FCS files were exported and analysed using FlowJo v10.7.2 (BD-Biosciences) software.

In vitro cytokine analysis

Frozen PBMCs were thawed and activated with phorbol 12-myristate 13-acetate (PMA; 50 ng/ml, Sigma-Aldrich) and Ionomycin (1µM, Sigma-Aldrich) for 5h at 37C. Inhibitor of intracellular protein transport, Brefeldin A (eBioscience), was added to cells at the start of stimulation. Cells incubated with vehicle (DMSO) and Brefeldin A were used as unstimulated controls. Cytokines production was analysed by flow cytometry. Briefly, cells were incubated with LIVE/DEAD fixable Aqua dead cell stain (Thermo Fisher Scientific) and Fc block, followed by cell-surface marker staining. Cells were then fixed and permeabilised using fixation/permeabilization buffer (BD Biosciences). Antibodies to stain intracellular cytokines were added and incubated for 30 min at room temperature. All samples were acquired on the BD LSRFortessa using FACSDIVA software (BD-Biosciences). FCS files were exported and analysed using FlowJo v10.7.2 (BD-Biosciences) software.

T cell cytokine production by ELISpot

Samples were assessed at day 105 after 2nd dose BNT162b2 immunisation. Frozen PBMCs were thawed and rested for 2-3 hours in RPMI media supplemented with 10% (v/v) Human AB Serum (Sigma) and 1% (v/v) Penicillin/Streptomycin (Sigma) at 37°C. Plates precoated with capture antibody (Mabtech, mAb 1-D1K) were washed three times with PBS and then blocked with supplemented RPMI media at 37°C for 1-2 hours. Overlapping peptide pools (18-mers with 10 amino acid overlap. Mimotopes) representing the spike (S),

medRxiv preprint doi: https://doi.org/10.1101/2022.09.17.22280033; this version posted February 22, 2023. The copyright holder for this preprint (which was not certified by peer review) is the author/funder, who has granted medRxiv a license to display the preprint in perpetuity. All rights reserved. No reuse allowed without permission.

Membrane (M) or nucleocapsid (N) SARS-CoV-2 proteins were added to 200,000 PBMCs/well at a final concentration of 2µg/ml. Concanavalin A (Sigma) was used as positive control. DMSO (Sigma) was used as the negative control at the equivalent concentration to the peptides. Plates were incubated at 37°C, for 18 hours. Wells were washed with PBS 0.05% (v/v) Tween (Sigma) seven times before incubation for 2 hours at room temperature with the ELISpot PLUS kit biotinylated detection antibody (clone 7-B6-1) at 1 µg/ml. Wells were washed and then incubated with the ELISpot PLUS kit streptavidin-ALP at 1µg/ml for 1 hour at room temperature. Wells were washed and colour development was carried out using 1-step NBT/BCIP Substrate Solution, for 5 minutes at room temperature. Colour development was stopped by washing the plates with cold tap water. Plates were left to air dry for 48 hours and then scanned and analysed using the AID iSpot Spectrum ELISpot reader (software version 7.0, Autoimmune Diagnostika GmbH, Germany). The average spot count of the control wells were subtracted from the test wells for each sample to quantify the antigen-specific responses. Results are expressed as spot forming units (SFU) per 106 PBMCs.

Statistical analysis

Statistical analysis for FACS and serology data was performed using GraphPad Prism v9.1.1 (GraphPad Prism Software Inc). Two-tailed non-parametric Mann Whitney tests were used to determine differences between groups. For multiple comparisons ANOVA with Tukey's multiple comparisons test was used. Associations were calculated using two-tailed Spearman's rank correlations and results are shown with linear trend levels. For the single cell data, statistical significance for paired comparisons were performed using Wilcoxon rank sum test in R.

Data and code availability

Sequencing data have been deposited in the Gene Expression Omnibus database [GEO: in preparation]. Additional information and materials and all codes for scRNA-seq analysis will be made available upon request.

Method references

1. Zheng, G.X., et al., Massively parallel digital transcriptional profiling of single cells. Nat Commun, 2017. 8: p. 14049.

2. Roelli, P., B. Flynn, and G. Gui, Hoohm/CITE-seq-Count: 1.5.0. . Zenodo, 2019.

3. Hao, Y., et al., Integrated analysis of multimodal single-cell data. Cell, 2021. 184(13): p. 3573-3587 e29.

medRxiv preprint doi: https://doi.org/10.1101/2022.09.17.22280033; this version posted February 22, 2023. The copyright holder for this preprint (which was not certified by peer review) is the author/funder, who has granted medRxiv a license to display the preprint in perpetuity. All rights reserved. No reuse allowed without permission.

4. McCarthy, D.J., et al., Scater: pre-processing, quality control, normalization and visualization of single-cell RNA-seq data in R. Bioinformatics, 2017. 33(8): p. 1179-1186.

5. Bhamidipati, K., et al., CD52 Is Elevated on B cells of SLE Patients and Regulates B Cell Function. Front Immunol, 2020. 11: p. 626820.

6. Ashburner, M., et al., Gene ontology: tool for the unification of biology. The Gene Ontology Consortium. Nat Genet, 2000. 25(1): p. 25-9.

7. Gene Ontology, C., The Gene Ontology resource: enriching a GOld mine. Nucleic Acids Res, 2021. 49(D1): p. D325-D334.

8. Mi, H., et al., PANTHER version 14: more genomes, a new PANTHER GO-slim and improvements in enrichment analysis tools. Nucleic Acids Res, 2019. 47(D1): p. D419-D426.

9. Stephenson, E., et al., Single-cell multi-omics analysis of the immune response in COVID-19. Nat Med, 2021. 27(5): p. 904-916.

10. Suo, C., et al., Dandelion utilizes single cell adaptive immune receptor repertoire to explore lymphocyte developmental origin. bioRxiv, 2023.

11. Gupta, N.T., et al., Change-O: a toolkit for analyzing large-scale B cell immunoglobulin repertoire sequencing data. Bioinformatics, 2015. 31(20): p. 3356-8.

12. Gadala-Maria, D., et al., Automated analysis of high-throughput B-cell sequencing data reveals a high frequency of novel immunoglobulin V gene segment alleles. Proc Natl Acad Sci U S A, 2015. 112(8): p. E862-70.

13. Bashford-Rogers, R.J., et al., Network properties derived from deep sequencing of human B-cell receptor repertoires delineate B-cell populations. Genome Res, 2013. 23(11): p. 1874-84.

14. Yamano, T., et al., Thymic B Cells Are Licensed to Present Self Antigens for Central T Cell Tolerance Induction. Immunity, 2015. 42(6): p. 1048-61.

15. Alquicira-Hernandez, J. and J.E. Powell, Nebulosa recovers single cell gene expression signals by kernel density estimation. Bioinformatics, 2021.

16. Xiong, X., et al., A thermostable, closed SARS-CoV-2 spike protein trimer. Nat Struct Mol Biol, 2020. 27(10): p. 934-941.

17. Collier, D.A., et al., Age-related immune response heterogeneity to SARS-CoV-2 vaccine BNT162b2. Nature, 2021. 596(7872): p. 417-422.

18. Stadlbauer, D., et al., SARS-CoV-2 Seroconversion in Humans: A Detailed Protocol for a Serological Assay, Antigen Production, and Test Setup. Curr Protoc Microbiol, 2020. 57(1): p. e100.

19. Daly, J.L., et al., Neuropilin-1 is a host factor for SARS-CoV-2 infection. Science, 2020. 370(6518): p. 861-865.

medRxiv preprint doi: https://doi.org/10.1101/2022.09.17.22280033; this version posted February 22, 2023. The copyright holder for this preprint (which was not certified by peer review) is the author/funder, who has granted medRxiv a license to display the preprint in perpetuity. All rights reserved. No reuse allowed without permission.

20. Moore, S.C., et al., Amplicon-Based Detection and Sequencing of SARS-CoV-2 in Nasopharyngeal Swabs from Patients With COVID-19 and Identification of Deletions in the Viral Genome That Encode Proteins Involved in Interferon Antagonism. Viruses, 2020. 12(10).

21. Patterson, E.I., et al., Methods of Inactivation of SARS-CoV-2 for Downstream Biological Assays. J Infect Dis, 2020. 222(9): p. 1462-1467.

22. Bergamaschi, L., et al., Longitudinal analysis reveals that delayed bystander CD8+ T cell activation and early immune pathology distinguish severe COVID-19 from mild disease. Immunity, 2021. 54(6): p. 1257-1275 e8.

23. Gerber, P.P., et al., A protease-activatable luminescent biosensor and reporter cell line for authentic SARS-CoV-2 infection. PLoS Pathog, 2022. 18(2): p. e1010265.

24. Knezevic, I., et al., WHO International Standard for evaluation of the antibody response to COVID-19 vaccines: call for urgent action by the scientific community. Lancet Microbe, 2022. 3(3): p. e235-e240.

25. Hedhammar, M. and S. Hober, Z(basic)--a novel purification tag for efficient protein recovery. J Chromatogr A, 2007. 1161(1-2): p. 22-8.

(which was not certified by peer review) is the author/funder, who has granted medRxiv a license to display the preprint in perpetuity.
All rights reserved. No reuse allowed without permission.

Figure 1

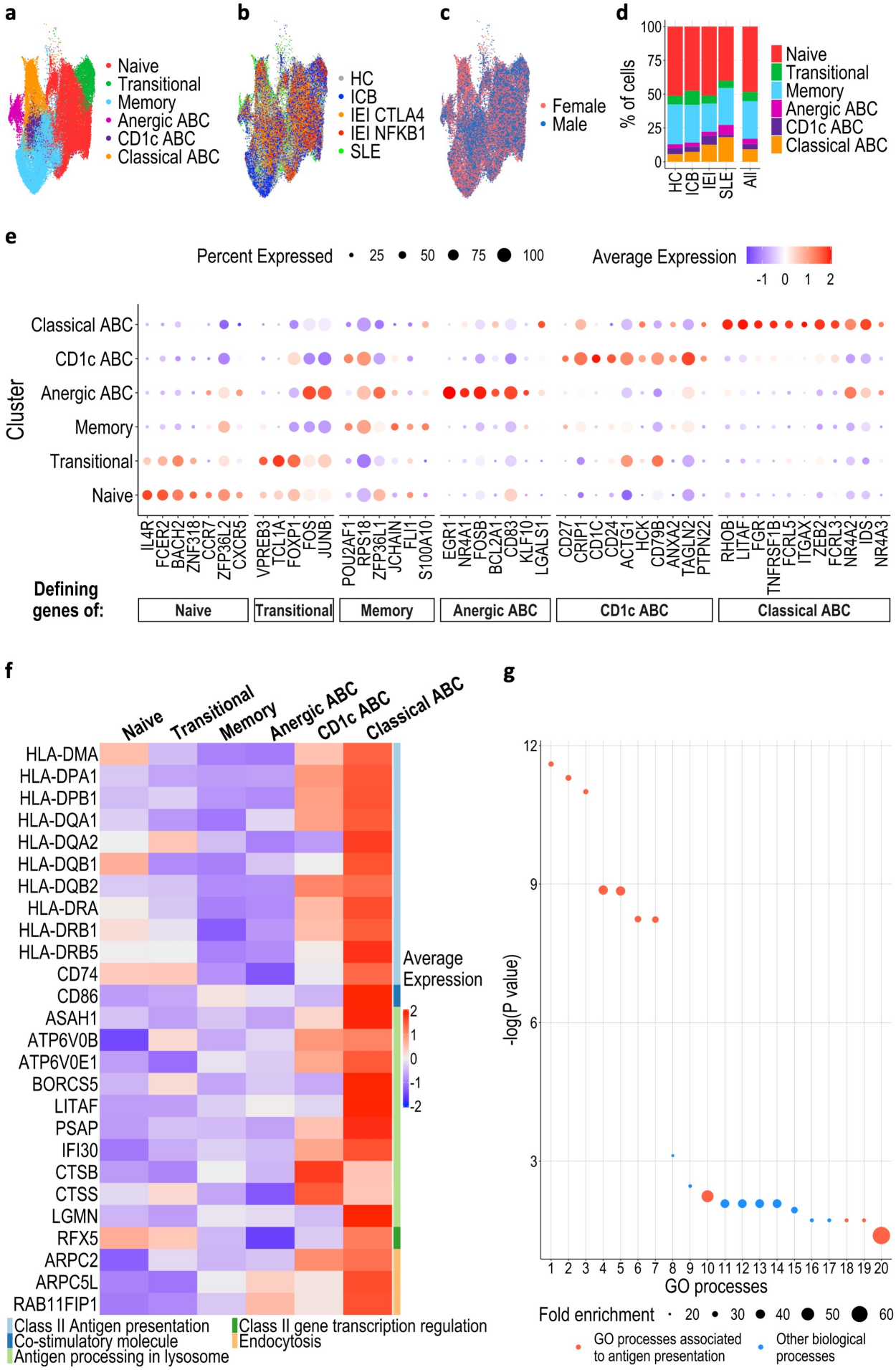

(which was not certified by peer review) is the author/funder, who has granted medRxiv a license to display the preprint in perpetuity.
All rights reserved. No reuse allowed without permission.

Supplementary Figure 1

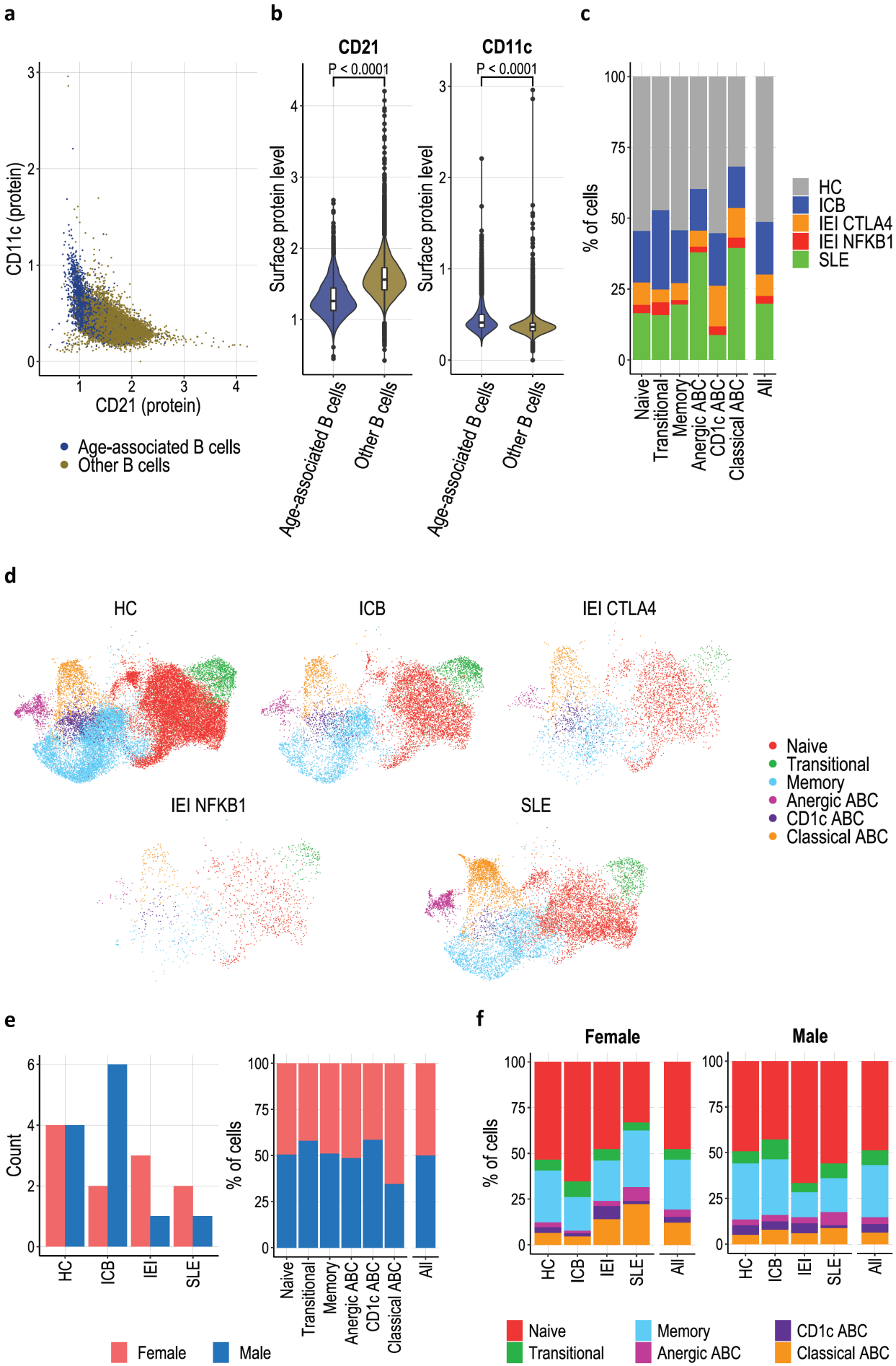

(which was not certified by peer review) is the author/funder, who has granted medRxiv a license to display the preprint in perpetuity.
All rights reserved. No reuse allowed without permission.

Supplementary Figure 2

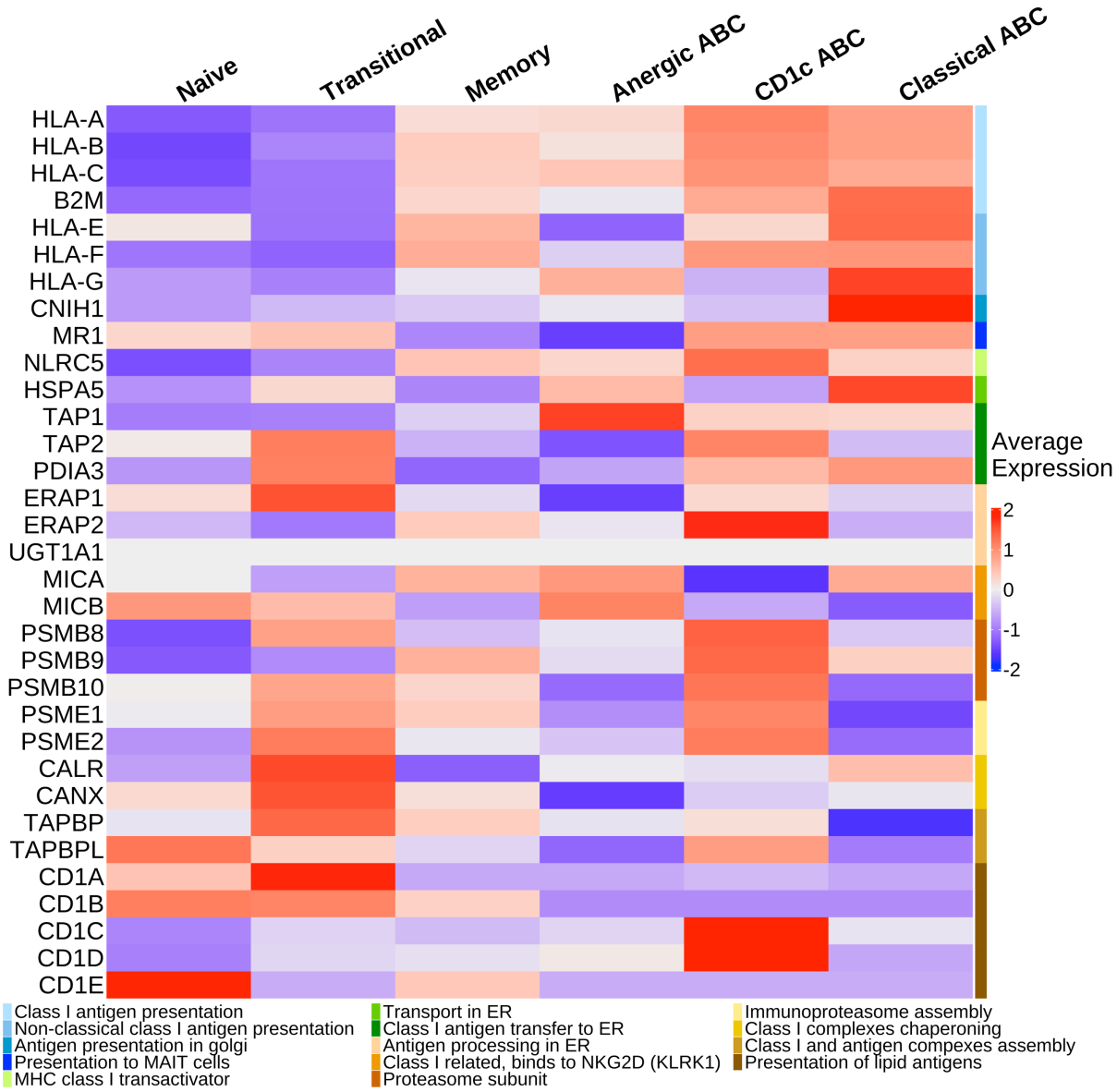

(which was not certified by peer review) is the author/funder, who has granted medRxiv a license to display the preprint in perpetuity.
All rights reserved. No reuse allowed without permission.

Supplementary Figure 3

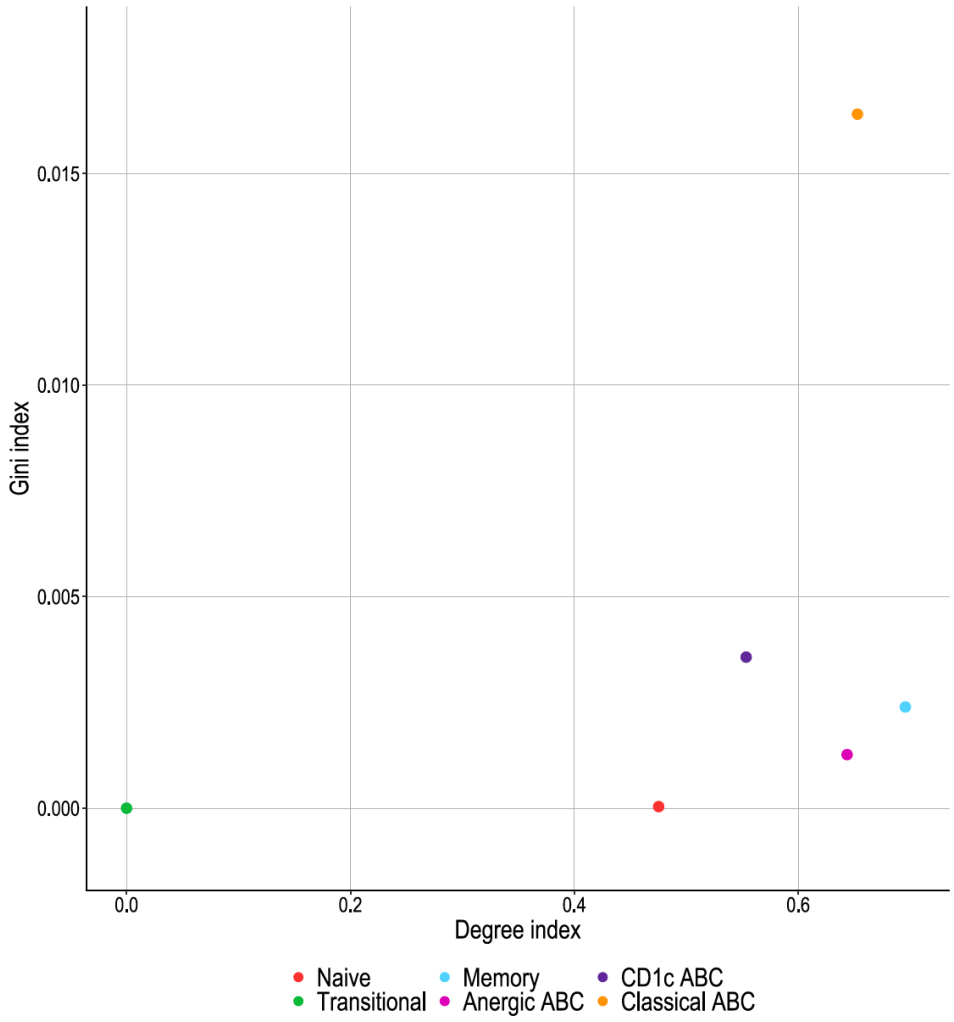

(which was not certified by peer review) is the author/funder, who has granted medRxiv a license to display the preprint in perpetuity.
All rights reserved. No reuse allowed without permission.

Figure 2

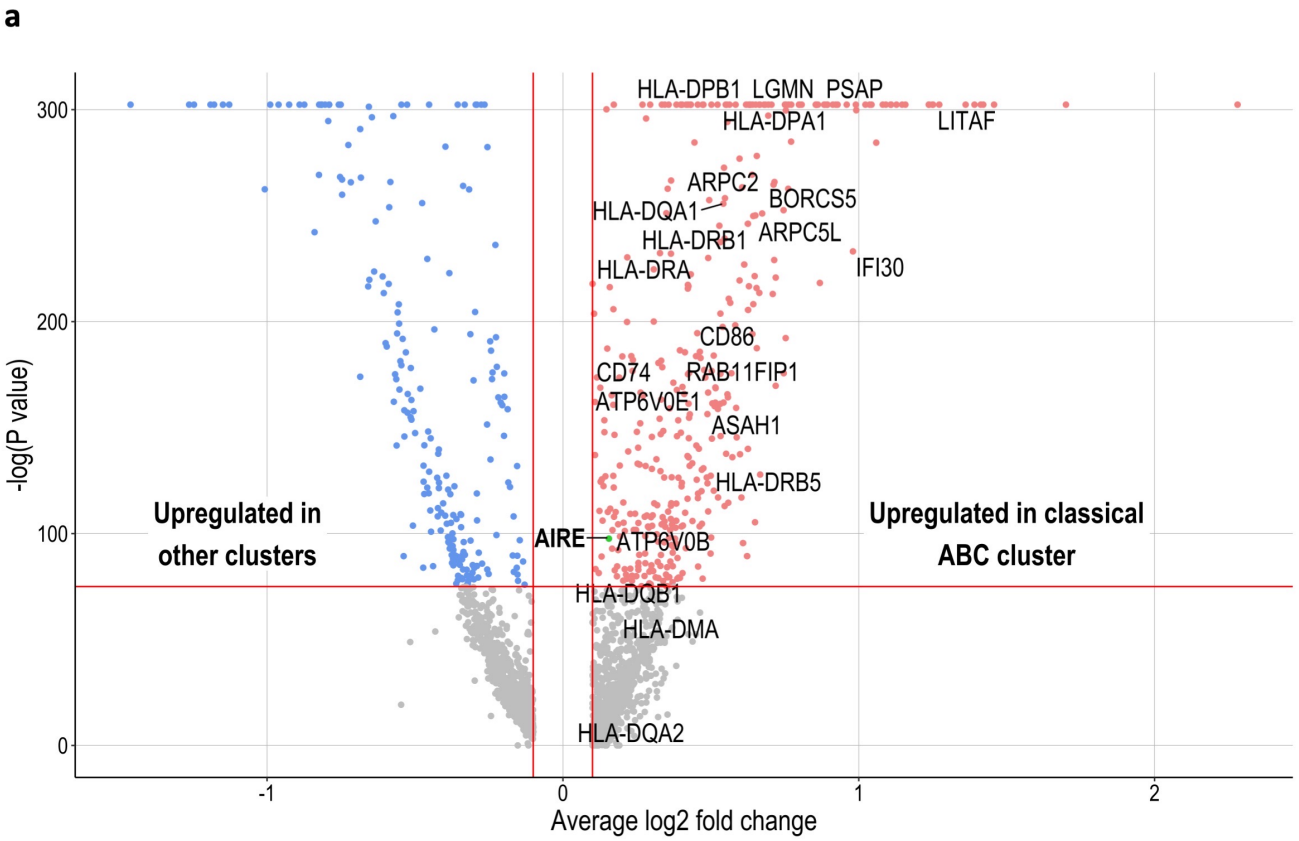

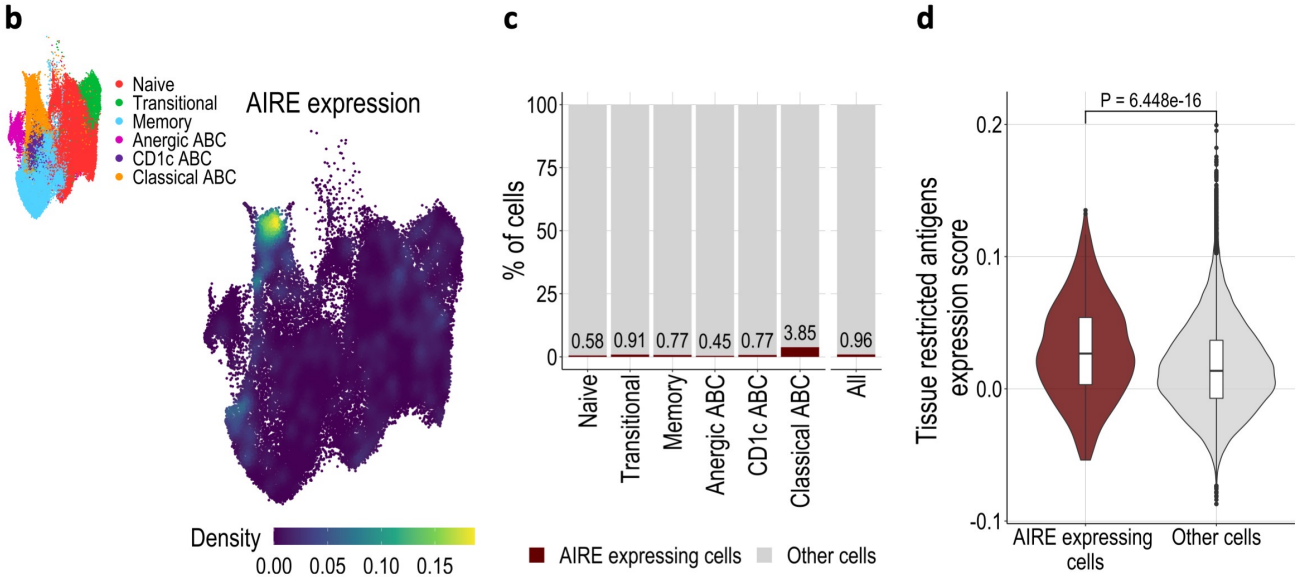

(which was not certified by peer review) is the author/funder, who has granted medRxiv a license to display the preprint in perpetuity.
All rights reserved. No reuse allowed without permission.

Supplementary Figure 4

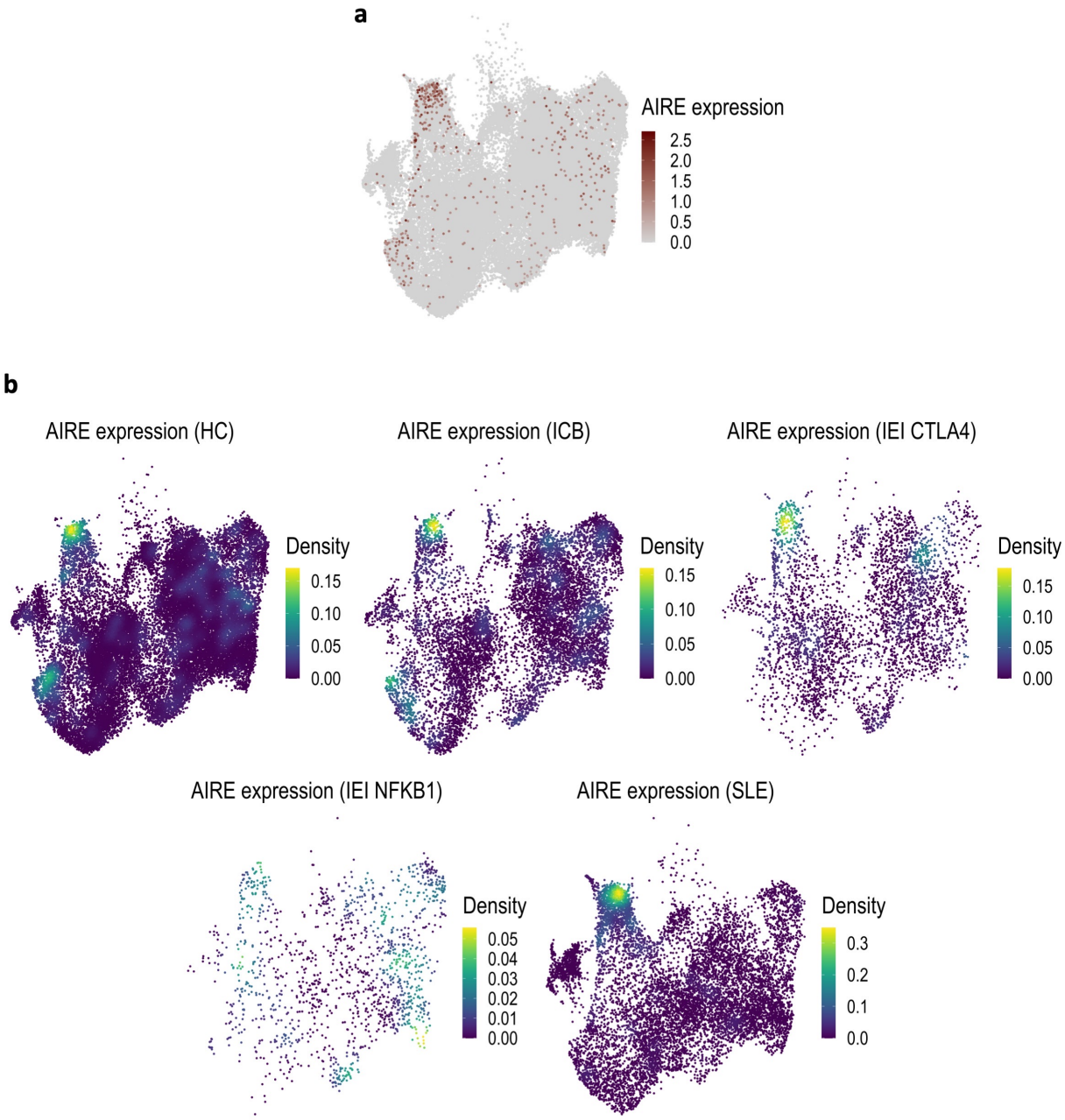

(which was not certified by peer review) is the author/funder, who has granted medRxiv a license to display the preprint in perpetuity.
All rights reserved. No reuse allowed without permission.

Supplementary Figure 5

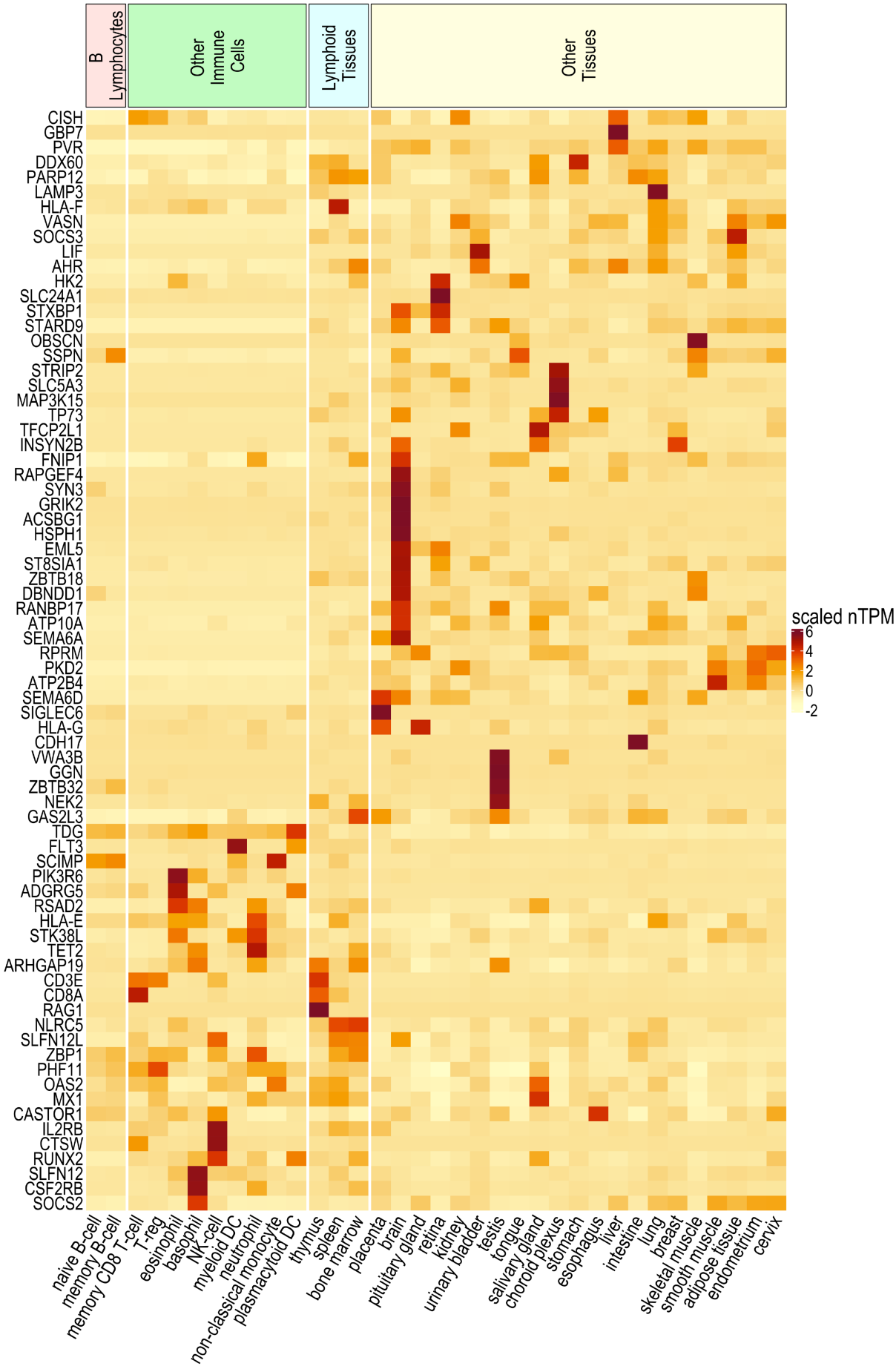

(which was not certified by peer review) is the author/funder, who has granted medRxiv a license to display the preprint in perpetuity.
All rights reserved. No reuse allowed without permission.

Figure 3

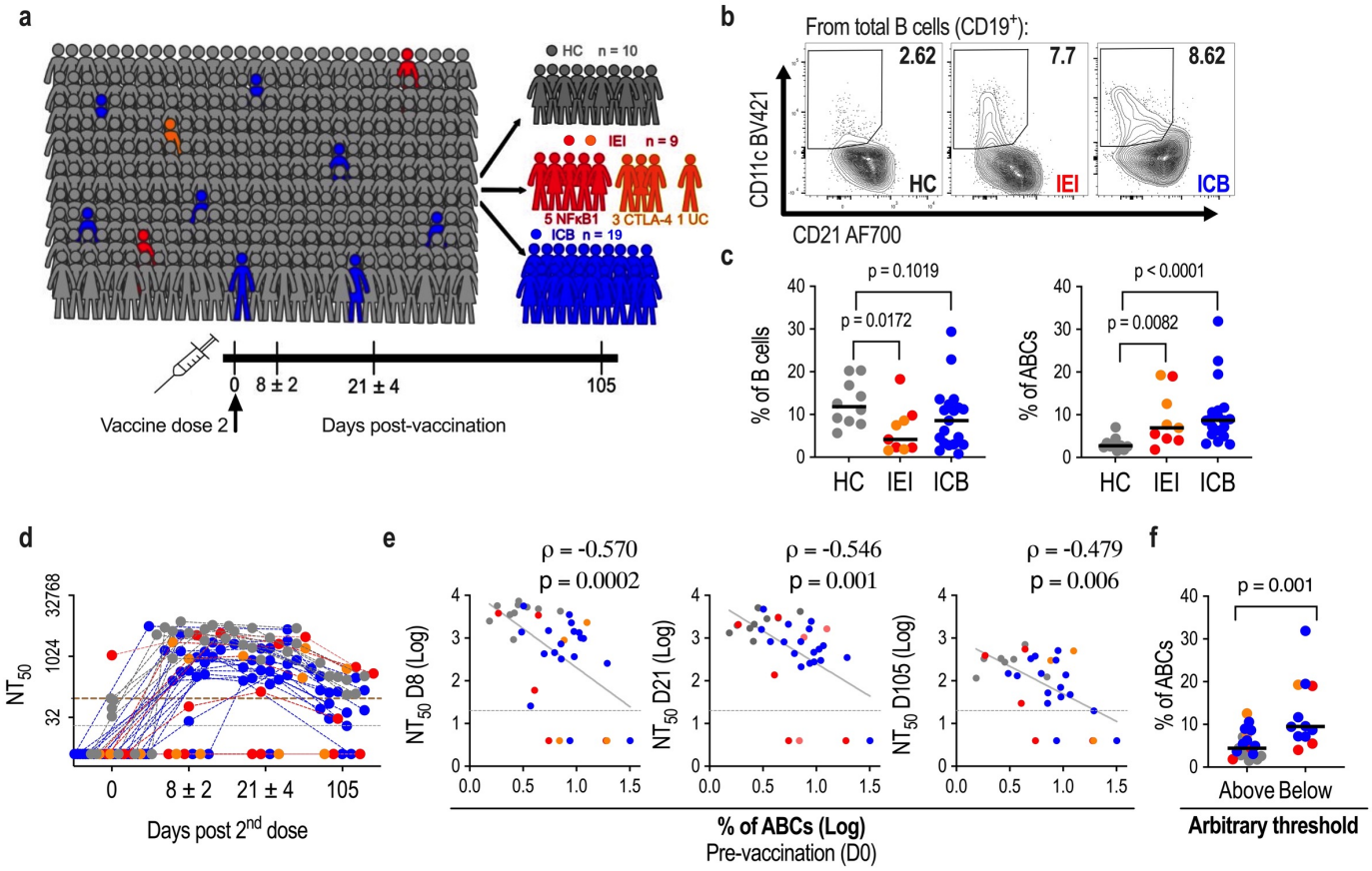

(which was not certified by peer review) is the author/funder, who has granted medRxiv a license to display the preprint in perpetuity.
All rights reserved. No reuse allowed without permission.

Supplementary Figure 6

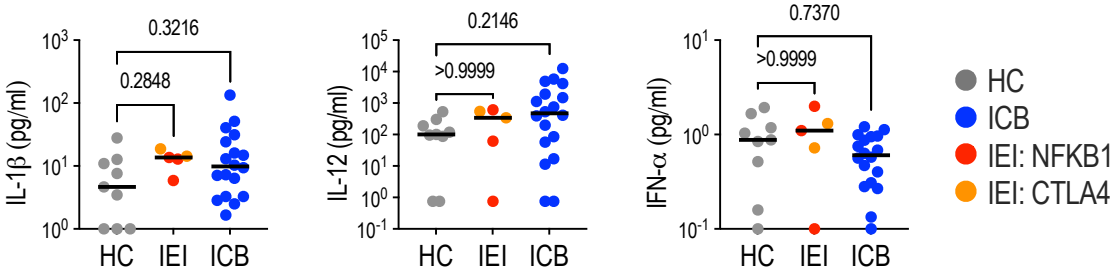

(which was not certified by peer review) is the author/funder, who has granted medRxiv a license to display the preprint in perpetuity.
All rights reserved. No reuse allowed without permission.

Supplementary Figure 7

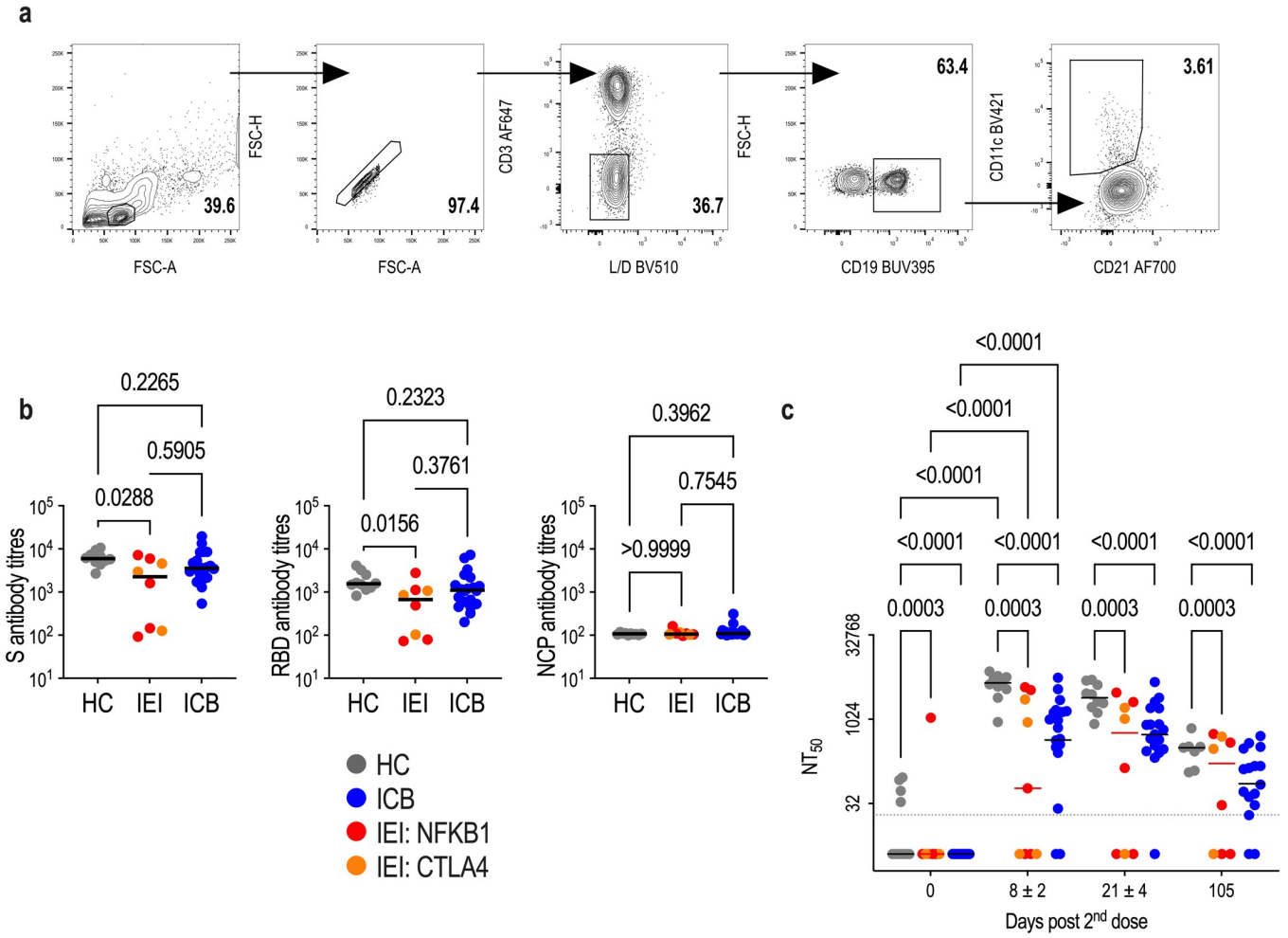

(which was not certified by peer review) is the author/funder, who has granted medRxiv a license to display the preprint in perpetuity.
All rights reserved. No reuse allowed without permission.

Supplementary Figure 8

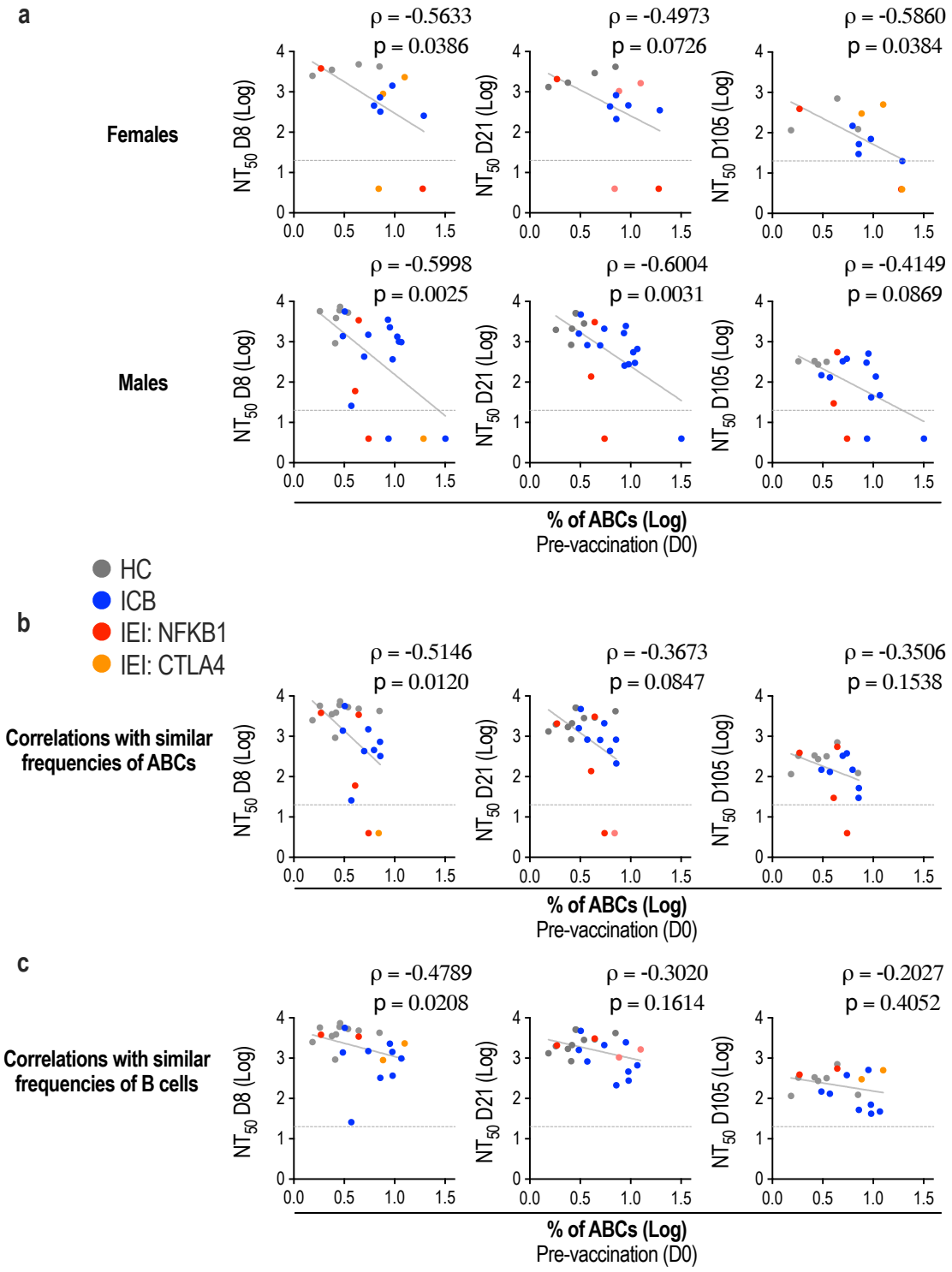

(which was not certified by peer review) is the author/funder, who has granted medRxiv a license to display the preprint in perpetuity.
All rights reserved. No reuse allowed without permission.

Figure 4

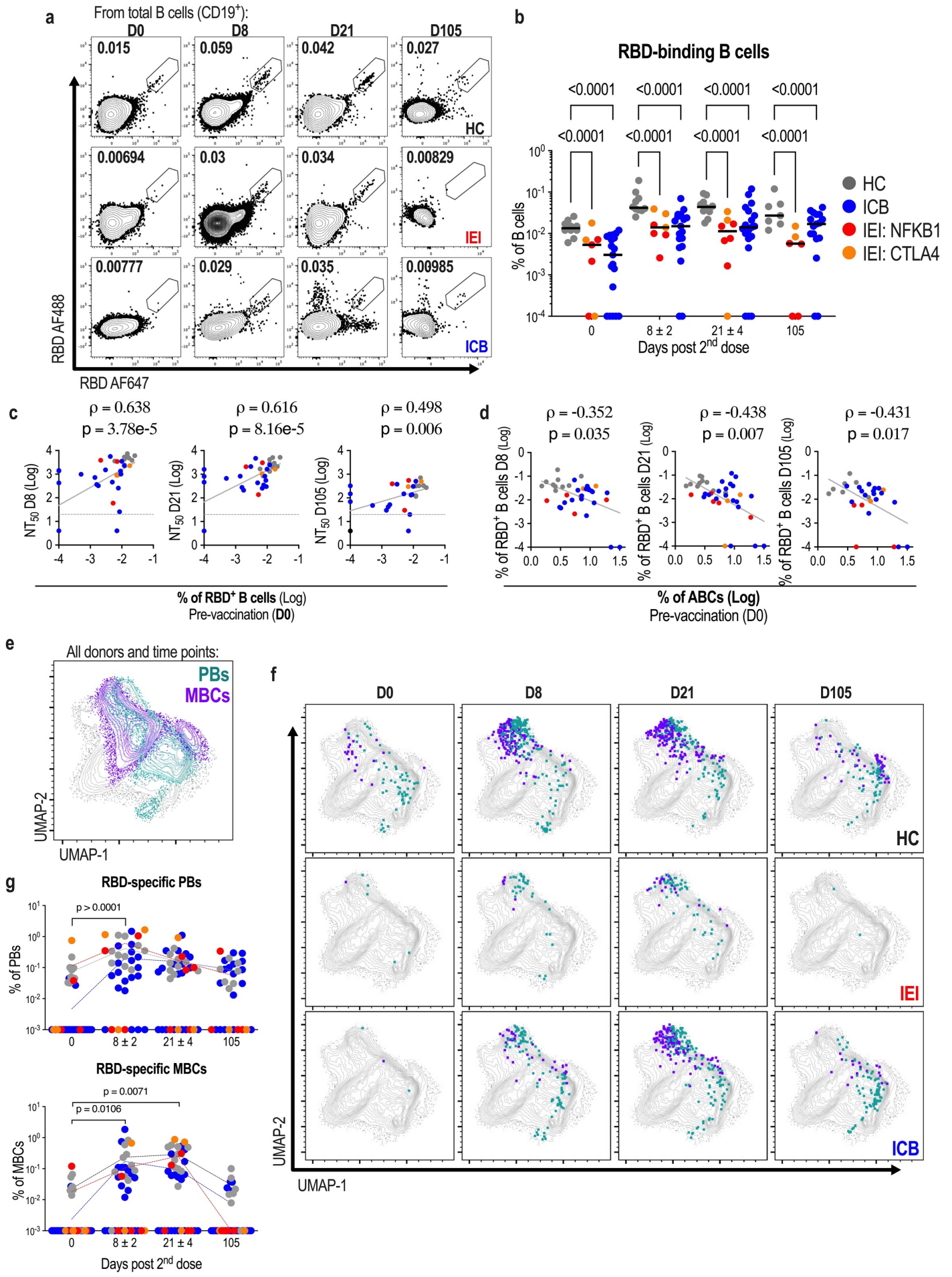

(which was not certified by peer review) is the author/funder, who has granted medRxiv a license to display the preprint in perpetuity.
All rights reserved. No reuse allowed without permission.

Supplementary Figure 9

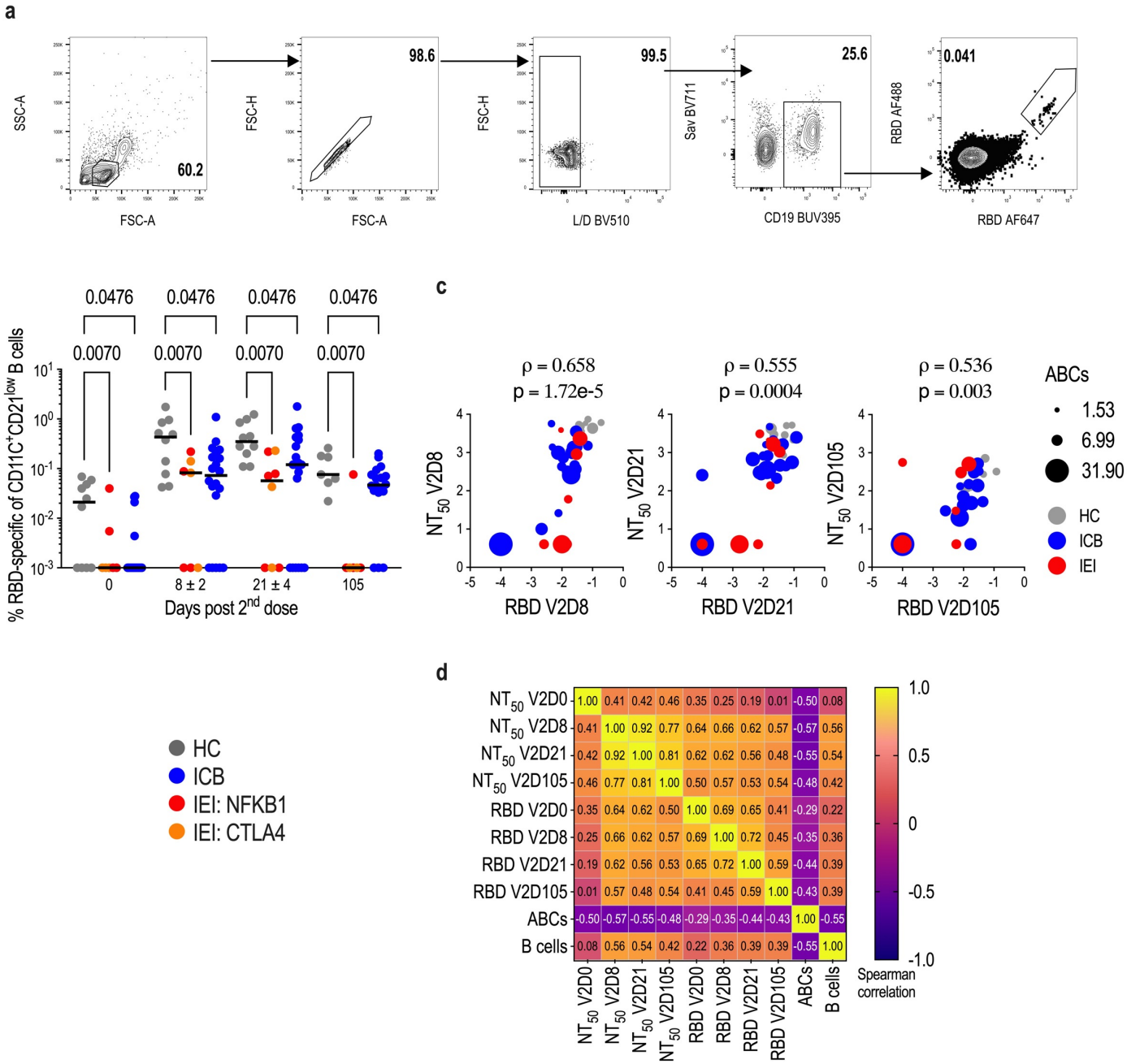

(which was not certified by peer review) is the author/funder, who has granted medRxiv a license to display the preprint in perpetuity.
All rights reserved. No reuse allowed without permission.

Supplementary Figure 10

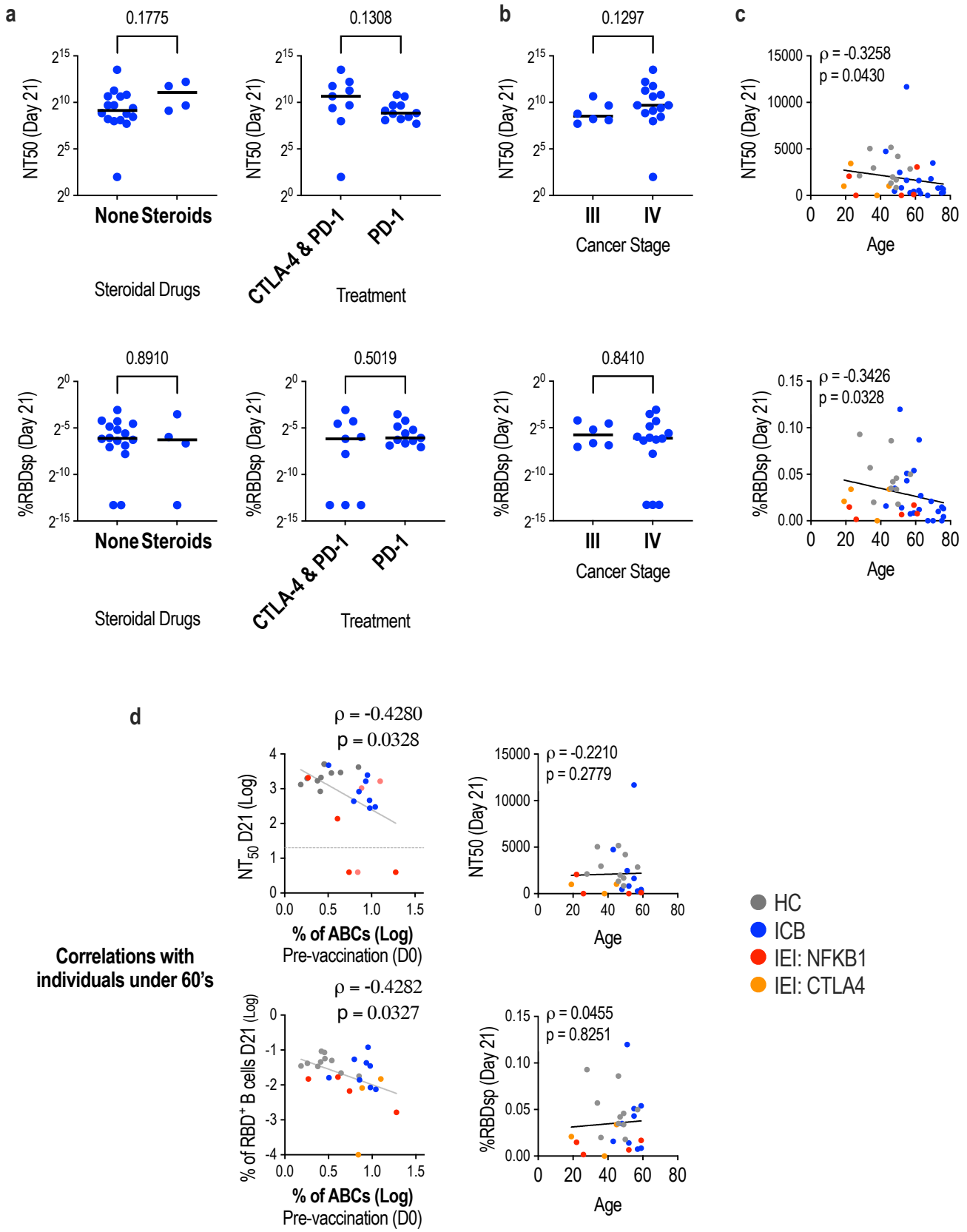

(which was not certified by peer review) is the author/funder, who has granted medRxiv a license to display the preprint in perpetuity.
All rights reserved. No reuse allowed without permission.

Supplementary Figure 11

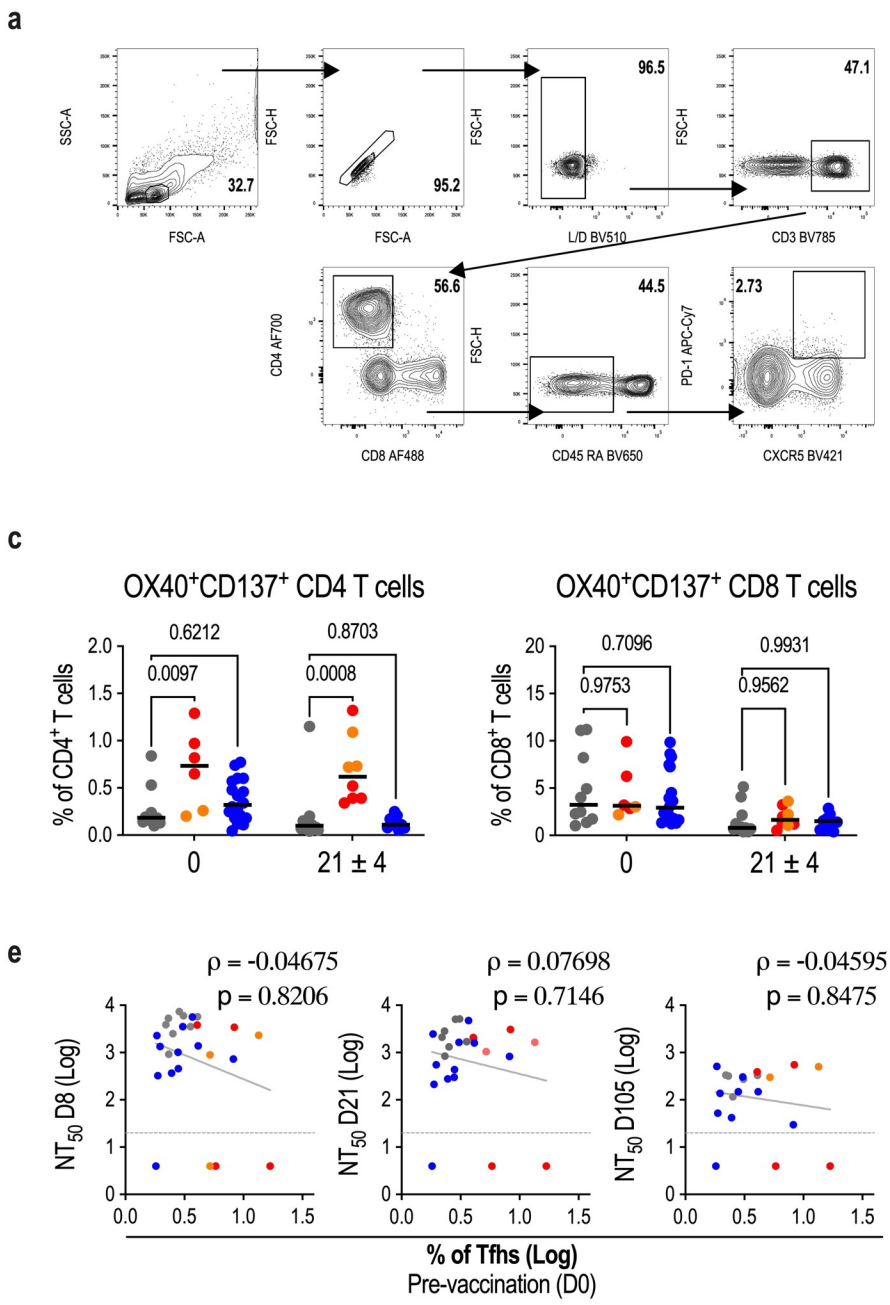

(which was not certified by peer review) is the author/funder, who has granted medRxiv a license to display the preprint in perpetuity.
All rights reserved. No reuse allowed without permission.

Figure 5

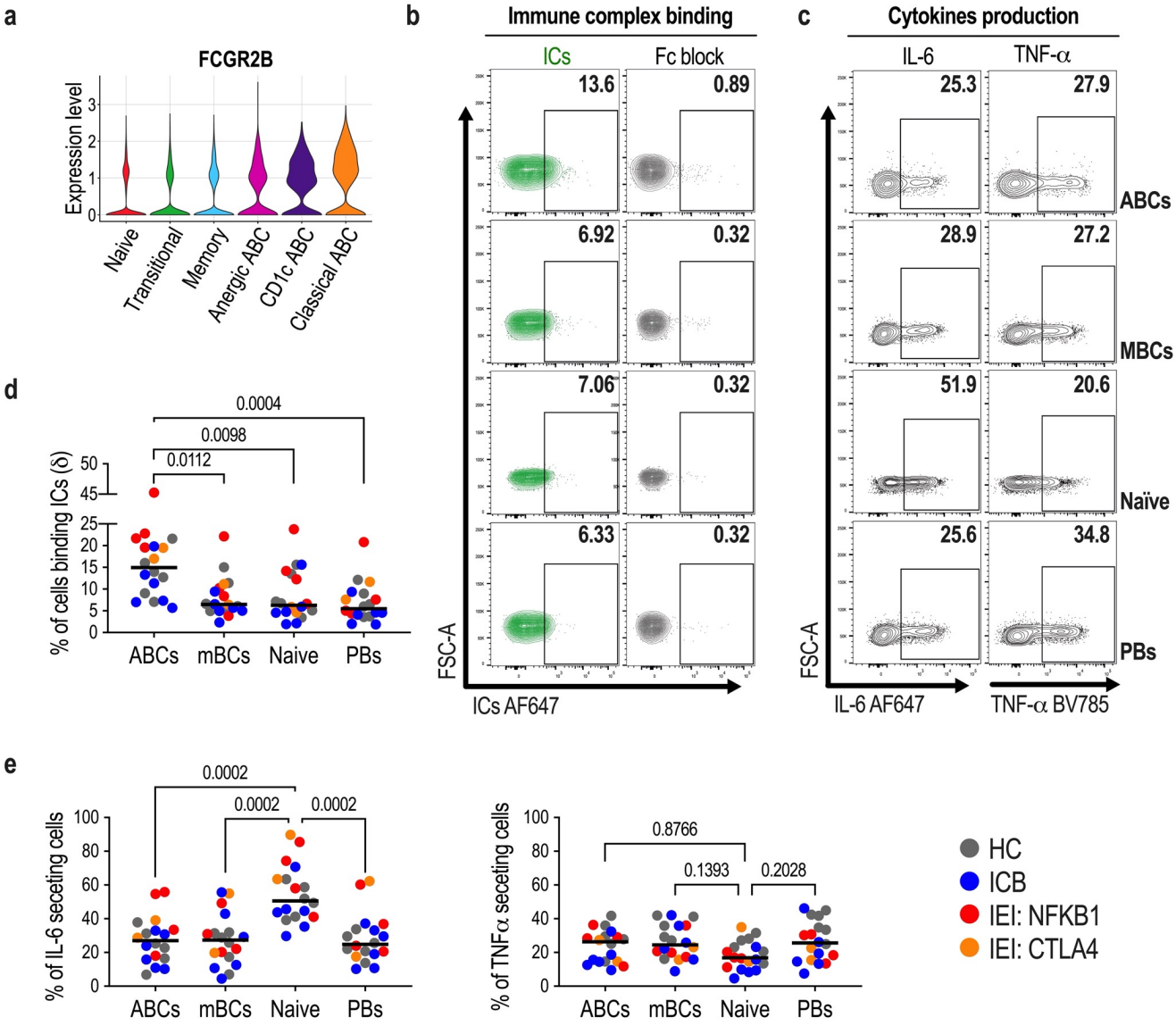

(which was not certified by peer review) is the author/funder, who has granted medRxiv a license to display the preprint in perpetuity.
All rights reserved. No reuse allowed without permission.
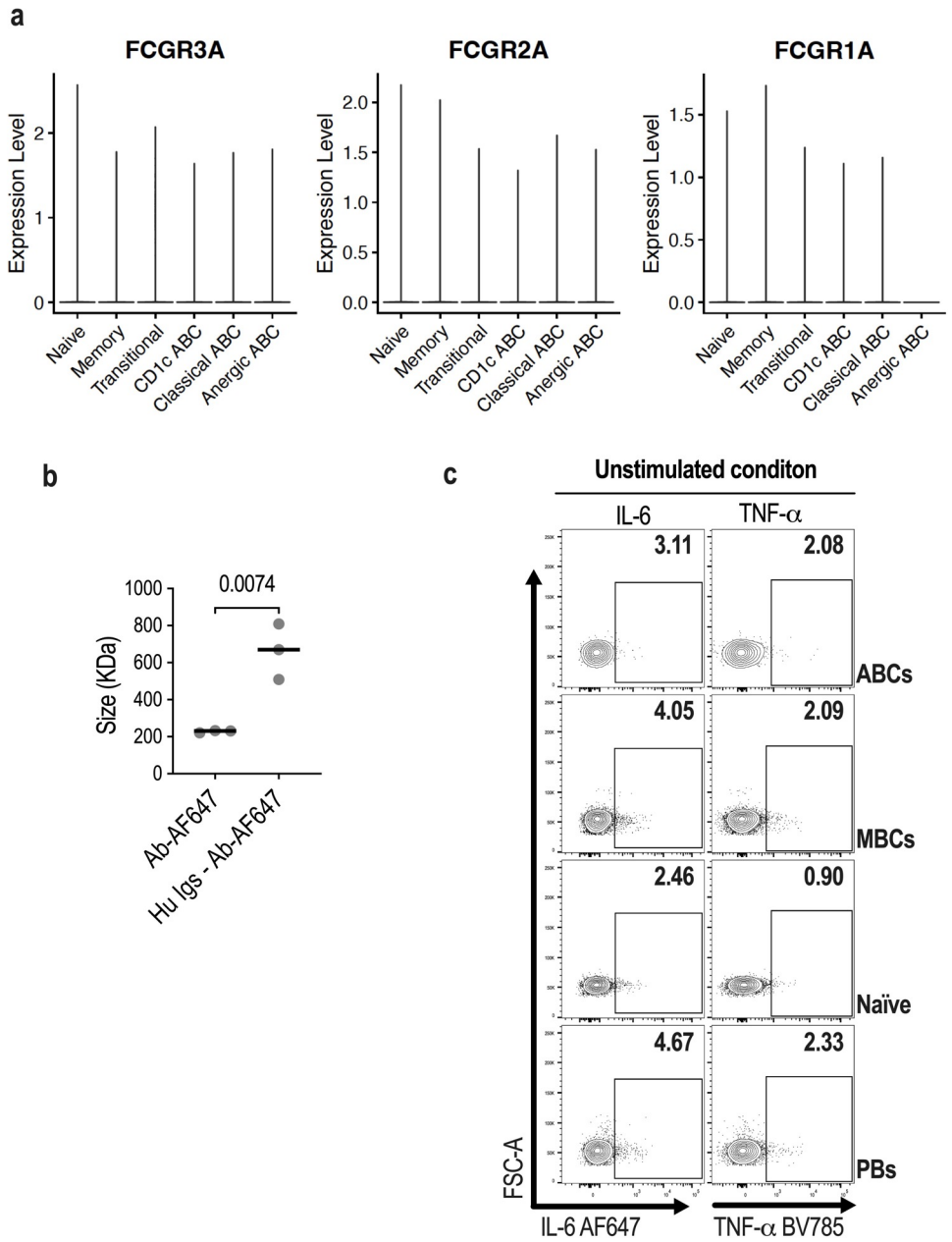
Supplementary Figure 12